Genome Methylation Predicts Age and Longevity of Bats

Gerald S. Wilkinson[1], Danielle M. Adams[1], Bryan D. Arnold[2], Hope C. Ball[3], Charles E. Breeze[4], Gerald Carter[5], Lisa Noelle Cooper[3], Dina K.N. Dechmann[6,7,8], Paolo S. Devanna[10], Nicolas J. Fasel[11], Alexander V. Galazyuk[3], Linus Gunther[12], Amin Haghani[13], Caesar Z. Li[14], Ake T Lu[13], Edward Hurme[1,6], Gareth Jones[15], Mirjam Knornschild[8,12], Ella Z. Lattenkamp[9,10], Frieder Mayer[12], Rodrigo A. Medellin[20], Martina Nagy[12], Brian Pope[21], Megan L. Power[19], Roger D. Ransome[15], Josephine A. Reinhardt[16], Emma C. Teeling[19], Sonja C. Vernes[10,17,18], Daniel Zamora-Mejías[20], Joshua Zhang[13], Joseph Zoller[14] and Steve Horvath[13,14]

1 *Department of Biology, University of Maryland, College Park 20742 USA*
2 *Department of Biology, Illinois College, Jacksonville, IL 62650 USA*
3 *Department of Anatomy and Neurobiology, Northeast Ohio Medical University, Rootstown, Ohio, U.S.A. 44272-0095*
4 *Altius Institute for Biomedical Sciences, Seattle, WA, 98121 USA*
5 *Department of Evolution, Ecology and Organismal Biology, The Ohio State University, 318 W. 12th Avenue, Columbus, OH, 43210 - 1293 USA*
6 *Department of Migration, Max Planck Institute of Animal Behavior, Radolfzell, Germany*
7 *Department of Biology, University of Konstanz, Konstanz, Germany*
8 *Smithsonian Tropical Research Institute, Panama*
9 *Department Biology II, Ludwig Maximilians University Munich, Martinsried, Germany*
10 *Neurogenetics of Vocal Communication Group, Max Planck Institute for Psycholinguistics, Nijmegen, The Netherlands*
11 *Department of Ecology and Evolution, University of Lausanne, Lausanne, Switzerland*
12 *Museum für Naturkunde, Leibniz-Institute for Evolution and Biodiversity Science, Berlin, Germany*
13 *Department of Human Genetics, David Geffen School of Medicine, University of California, Los Angeles USA*
14 *Department of Biostatistics, Fielding School of Public Health, University of California, Los Angeles USA*
15 *School of Biological Sciences, University of Bristol, Bristol, UK*
16 *Department of Biology, State University of New York, Geneseo USA*
17 *Donders Institute for Brain, Cognition and Behaviour, Nijmegen, The Netherlands*
18 *School of Biology, The University of St Andrews, Fife, UK*
19 *School of Biology and Environmental Science, University College Dublin, Belfield, Dublin 4, Ireland*
20 *Instituto de Ecología, Universidad Nacional Autónoma de México, Ap. Postal 70-275 04510, Ciudad Universitaria, México*
21 *Lubee Bat Conservancy, 1309 NW 192nd Avenue, Gainesville, FL 32609 USA*

Correspondence: GSW (wilkinso@umd.edu) and SH (shorvath@mednet.ucla.edu)

Summary

Bats hold considerable potential for understanding exceptional longevity because some species can live eight times longer than other mammals of similar size [1]. Estimating their age or longevity is difficult because they show few signs of aging. DNA methylation (DNAm) provides a potential solution given its utility for estimating age [2-4] and lifespan [5-7] in humans. Here, we profile DNAm from wing biopsies of nearly 700 individuals representing 26 bat species and demonstrate that DNAm can predict chronological age accurately. Furthermore, the rate DNAm changes at age-informative sites is negatively related to longevity. To identify longevity-informative sites, we compared DNAm rates between three long-lived and two short-lived species. Hypermethylated age and longevity sites are enriched for histone and chromatin features associated with transcriptional regulation and preferentially located in the promoter regions of helix-turn-helix transcription factors (TFs). Predicted TF binding site motifs and enrichment analyses indicate that age-related methylation change is influenced by developmental processes, while longevity-related DNAm change is associated with innate immunity or tumorigenesis genes, suggesting that bat longevity results, in part, from augmented immune response and cancer suppression.

Aging of wild animals typically requires long-term mark-recapture data or lethal tissue sampling [8]. For long-lived animals, such as bats, these methods limit possible studies. An accurate, noninvasive aging method would enable study of chronological changes in traits critical for survival, such as sensory perception, metabolic regulation, and immunity. With species from multiple lineages capable of living over 30 years [1] despite tolerating high viral loads [9, 10], bats could provide insight into mechanisms that reduce deleterious aging

effects. Therefore, to determine if age in bats can be predicted by DNAm we used a custom microarray that assays 37,500 conserved cytosine-phosphate-guanine (i.e. CpG) sites to measure DNAm extracted from wing biopsies of 694 known-aged individuals representing 26 species of bats (Supplementary Table 1). Similar to human epigenetic clocks [4, 7], elastic-net regression accurately predicted chronological age from a linear combination of DNAm beta values (henceforth DNAmAge) using 150 CpG sites. Leave-one-out (LOO) cross-validation shows that DNAm predicts age accurately (Fig.1a). Even more accurate age estimation is possible for species (or genera) with sufficient data. For example, the correlation between observed and DNAmAge in a LOO cross-validation analysis of 40 *Pteropus hypomelanus* individuals is 0.98 (MAE = 0.63); a similar analysis on 176 samples from six *Pteropus* species gave a correlation of 0.97 (Supplementary Figs. 1, 2). Thus, DNAm from a wing tissue sample for any of these species can reveal the animal's age at the time of sampling to within a year.

To assess how well DNAm might predict age in a species not represented by our samples, we conducted a second cross-validation analysis in which data for one species was left out (leave-one-species out; LOSO) and ages were predicted for that species using a clock estimated from the remaining data. This analysis (Fig. 1b) resulted in a correlation between observed and predicted age of 0.8 (MAE=1.3 years). The LOSO analysis also showed that species vary in DNAmAge estimates. For example, *Desmodus rotundus* (sp. 5, Fig. 1b) exhibit lower values of DNAmAge (suggesting lower aging rates) than *Phyllostomus hastatus* (sp. 15, Fig. 1b), consistent with the longer lifespan of *D. rotundus* [1]. Experimental [11, 12] and observational data [13] suggest that DNAm rate varies with lifespan in model organisms.

However, interspecific studies have so far used different methods on a few primate, rodent, or canid species [12, 13] making it difficult to determine reasons for methylation differences.

Thus, to determine if DNAm rate predicts bat longevity, we incorporated a recent bat phylogeny [14] into a generalized least squares regression (PGLS) to predict the longevity quotient - the ratio of observed to expected maximum lifespan for a mammal of the same body size [1]. We identified a common set of CpG sites for this analysis by first conducting a meta-analysis of all age-DNAm correlations by probe for 19 bat species with 15 or more samples (Methods). We find that mean DNAm rate at 2000 age-associated sites (henceforth, age differentially methylated positions or age DMPs) predicts longevity. Long-lived species have lower rates of change at hypermethylated (Fig. 2a) and hypomethylated sites (Fig. 2b). Assuming that the rate of change in DNAm reflects epigenetic stability, these results suggest that better epigenetic maintenance is associated with longer maximum lifespan, independent of body size, across bats.

The distribution and function of genomic regions that exhibit age or longevity-related changes in DNAm are not fully understood [7, 15]. To identify DMPs associated with longevity, we compared relationships between DNAm and age for three long-lived species and two short-lived species (Fig. 2) from four bat families (Methods). After adjusting for multiple testing (BY FDR = 0.05, [16]), we identified 1491 longevity DMPs, including 694 in which short-lived species gain DNAm faster with age and 797 in which short-lived species lose DNAm faster. In the following, we refer to these sites as longevity DMPs. Both longevity and age DMPs are widely distributed in the genome, but differ in relative abundance across chromosomes (Fig. 3a,b). For example, of the 1228 probes that map to chromosome 1 (syntenic with the human X chromosome) in *R. ferrumequinum* (the bat genome with the most

mapped probes, 34,411, Supplementary Table 3) only 13 are age-associated while 61 are longevity-associated. Not surprisingly, 672 of 838 sites (80.2%) that differ between the sexes in methylation values are on the *R. ferrumequinum* X. Sex DMPs are independent of age DMPs (6.1% overlap, P = 0.25, Fisher's Exact Test, FET) but not longevity DMPs (5.8% overlap, P = 0.0064, FET). Age DMPs are also not independent of longevity DMPs (22.5% overlap, P < 0.0001, FET, Fig. 3c). Change in DNAm with respect to age correlates with change in DNAm with respect to longevity (r = 0.462, P < 0.0001); when limited to promoter regions, almost all DMPs exhibit hypermethylation and mapped to the same gene in multiple bat genomes (Fig. 3e).

The gene nearest each CpG site often differs between bats and humans (Fig. 4a). In contrast, genomic regions occupied by DMPs are similar among bat species (Supplementary Fig. 3). For example, 70% of 3197 probes that map to a promoter region in *M. molossus* map to a promoter region in *R. ferrumequinum* (Fig. 4b). Promoter regions in *M. molossus* (and other bats, Supplementary Fig. 4) are enriched for hypermethylating, but not hypomethylating, age and longevity DMPs (Fig. 4c,d). In bat genomes where CpG islands have been identified, hypermethylating DMPs are much more likely than hypomethylating DMPs to be located in CpG islands for the age (P < 0.0001, FET) and longevity (P < 0.0001, FET) associated sites.

Given that regions near promoters contain more age and longevity DMPs than expected, we evaluated the genes nearest those DMPs for possible functions. In *M. molossus*, 36% of genes had DMPs associated with age and longevity (Fig. 3d). Other bats show similar patterns (Supplementary Fig. 4d). Not surprisingly, *M. molossus* genes with age or longevity DMPs in promoter regions show similar patterns of enrichment among biological processes,

i.e. regulation of development, biosynthetic processes, and regulation of transcription are enriched (Fig. 4e). Genes with age DMPs in promoter regions are further enriched for cell differentiation and cellular development. With regard to protein class, gene lists for both age and longevity DMPs are enriched for homeodomain transcription factors containing helix-turn-helix motifs (Fig. 4f). These patterns are characteristic of other bat species (Supplementary Fig. 5), although the gene list composition varies. For example, the same gene was near a hypermethylated site in a promoter region for 92 out of 143 age-associated genes in at least three of the four bat genomes used for identifying longevity DMPs. Additionally, hypermethylated age genes in bats strongly overlap hypermethylated age genes reported for dogs [18] (e.g. 60 of 316 genes for *M. molossus,* P = 7.79e-36, FET). In contrast, among hypomethylated age genes, only four of 353 *M. molossus* genes overlap with dog genes (P = 0.202, FET). Bat age genes include more immunity genes (Fig. 4g) than expected (P = 0.021, FET), but overlap between immunity and longevity genes is far greater (P = 0.001, FET). Bat longevity genes also overlap genes frequently mutated in human tumors (Fig. 4g, P = 0.025, FET), but bat age genes do not (P = 0.792, FET). Similar overlap patterns among immunity, longevity and tumor mutated genes occur for other bats (Supplementary Fig. 5).

Gene promoters poised for transcription can be identified by histone marks and chromatin states [19]. Given that hypermethylation associated with human aging occurs at bivalent chromatin domains [20], we used eFORGEv.2.0 [21] to predict how DMPs likely influence regulatory regions based on epigenetic studies in human or mouse cell lines derived from relevant tissues. We find that sites exhibiting hypermethylation with age and longevity in bat wing tissue are enriched for repressive histone H3 trimethylated at lysine27

(H3K27me3) and active H3K4me1 marks in skin, muscle and blood cell lines (Fig. 5a, b). Hypomethylated age DMPs are enriched in all three tissues for H3K9me3, while hypomethylated longevity DMPs show no enrichment (Fig. 5a, b). Analysis of predicted chromatin states reveals that hypermethylated age DMPs are enriched in all three tissues for repressed polycomb complexes, while hypomethylated age DMPs are enriched for quiescent chromatin states (Fig. 5c). Longevity DMPs, both hypermethylating and hypomethylating, also show enrichment for quiescent states, as well as enrichment for repressive polycomb complexes or enhanced bivalent states in some tissues (Fig. 5d).

Transcription factor (TF) motifs involved in cell cycle regulation and genome stability are enriched among hypermethylating age sites (Fig. 5e). Several of those transcription factors, including cut-like homeobox 1 (CUX1), AT-rich interaction domain 3A (ARID3), and E2F transcription factor 1 (E2F) are involved in cell cycle regulation [22-24], while others, such as zinc finger protein 161 (ZFP161), are involved in genome stability [25]. In contrast, hypomethylating age sites only overlap with three TF clusters, one of which, IRF7, is a master regulator of the interferon-dependent innate immune response in bats [26].

Longevity TF motifs are largely independent of age TF motifs (Fig. 5e), with one exception, c203-transcription factor AP-2 gamma (TFAP2C), which is involved in epidermal cell lineage commitment [27] and regulation of tumor progression [28]. The other longevity TF motifs also have known associations with tumorigenesis. GCM1/3 binds to pleiomorphic adenoma gene-like 1 (Plagl1), which codes for a protein that suppresses cell growth. This gene is often methylated and silenced in cancer cells [29, 30]. CNOT3 acts as a tumor suppressor in T-cell acute lymphoblastic leukemia (T-ALL) [31] but can also facilitate development of non-small cell lung cancer [32]. Finally, HIC1, hypermethylated in cancer 1

protein, acts as a tumor suppressor and is involved in regulation of p53 DNA damage responses [33, 34]. Only a single TF motif, HD/5 in the BARHL2 group [35], was associated with hypomethylated longevity DMPs.

Enrichment analyses [36], using the age and longevity DMPs found in promoter regions to create gene lists for *M. molossus,* identify several key regulators that are significantly associated with hypermethylated sites, but none with hypomethylated sites (Fig. 5f and Supplementary Fig. 5c) Orthodenticle homeobox 2 (OTX2) is associated with both age and longevity, whereas other predicted TFs largely differ between age and longevity. The highest-ranked age TF, RE1 silencing transcription factor (REST), is induced during human aging and represses neuronal genes that promote cell death [37]. Note that four of nine transcription regulators predicted to be associated with longevity frequently undergo mutations in human tumors and three are involved in innate immunity (Fig. 5f).

DNAm influences many processes including development [38], gene regulation [39], genomic imprinting [40], X chromosome inactivation [41], transposable element defense [42], and cancer [43]. Over 75% of CpG sites are typically methylated in mammalian cells, but global DNAm declines with age, which can lead to loss of transcriptional control and either cause or contribute to deleterious aging effects [44]. As with other species [18, 45-47], age-related changes in DNAm occur throughout bat genomes. While only 150 CpG sites are sufficient to predict chronological age, these represent only a fraction of sites that correlate with age, because penalized regression excludes highly correlated variables to avoid multi-collinearity. Consequently, we carried out a marginal analysis that correlated individual cytosines with age across species to identify age DMPs. At these sites, long-lived species exhibit a lower rate of change in DNAm, while short-lived species exhibit faster increases in

DNAm. How those changes contribute to longevity is not entirely clear, but our results suggest several key transcriptional regulators are involved either by binding to DNA at open chromatin or by being enriched among genes with DMPs in promoter regions and modulate the rate at which DNAm changes between short and long-lived species.

Our results are consistent with an epigenetic clock theory of aging that connects beneficial developmental and cell maintenance processes to detrimental processes causing tissue dysfunction [7]. A large body of evidence links age-related hypermethylated sites to genes and genomic regions that influence developmental processes [18, 20, 48]. The sites that gain DNAm with age also tend to be in CpG islands, consistent with studies in humans [49]. But, in contrast, we find little enrichment for genes associated with hypomethylated sites, and these genes are less likely to be shared across species. We interpret these results to indicate that DNAm loss with age is widespread and not concentrated in particular pathways. These DNAm patterns could differ by tissue, as has been frequently observed [50]. However, bat wing tissue is capable of unusually rapid regeneration [51, 52] and consists of multiple tissue types [53], making it particularly useful for measuring age-related changes in DNAm.

DNAm of genes suppressed in stem cells is a hallmark of cancer [48]. Several lines of evidence suggest that bat genes with longevity DMPs are important for cancer suppression and provide enhanced immunity. First, these genes disproportionately include many known to mutate frequently in human cancers or involved in innate immunity. Second, several transcription factors identified by motif analysis act as tumor suppressors, such that if they are silenced by methylation in older individuals, tumor formation should be more likely. Third, among the transcription factors identified from the list of genes with hypermethylated sites in promoter regions, several of them mutate in human cancers. While bats are not immune from

cancer [54-59], genetic adaptations for tumor suppression have been described for *Myotis brandtii* [60] and *M. myotis* [61] to help explain the extreme longevity of those species. Bats also have genetic mechanisms that enable strong antiviral immune responses without inducing damaging inflammatory reactions (e.g. cytokine storm [62]) that may enable them to tolerate high levels of viral exposure [9, 10, 17, 63, 64]. The results of this study are consistent with the hypothesis that enhanced epigenetic stability, especially associated with innate immunity and cancer suppression genes, facilitates the exceptional longevity in bats.

Methods

Wing tissue samples

The number of tissue samples per species and per sex, as well as the range of ages of individuals of each bat species, are provided in Supplementary Table 1. Wing punches were taken from individually marked animals that were either kept in captivity (15 species) or recaptured as part of long-term field studies (11 species). For 652 samples the individual was marked shortly after birth, so age estimates were exact. For the remainder, age represented a minimum estimate because the individual was not initially banded as a juvenile. We used minimum age estimates when other evidence, such as tooth wear or time since initial capture, indicated that the minimum age estimate was likely to be close to the real age. Below, we provide additional information on when and where samples were taken from either captive or free-ranging animals.

Pallid bats, *Antrozous pallidus,* were captured between 2005 and 2008 at six sites in central Oregon (44.94°N, 120.38°W) using mist nets over a water source or outside a night roost or with a handnet on an extension pole outside a day-roosting crevice. Each bat was

weighed, measured and marked with a numbered band. Adults were distinguished from juveniles by closed epiphyseal gaps [8]. Tissue samples were obtained from wing membranes using 3 mm biopsy punches and stored in 95% ethanol until DNA was extracted using a Qiagen DNeasy Tissue Kit. DNA extracts were stored frozen at -80°C. Live animal procedures conformed to the American Society of Mammalogists guidelines [65] and were approved by the University of Maryland Institutional Animal Care and Use Committee (protocol R-08-39).

Wing tissue from *Artibeus jamaicensis, Cynopterus brachyotis, Eidolon helvum, Pteropus giganteus, P. hypomelanus, P. poliocephalus, P. pumilus, P. rodricensis, P. vampyrus, and Rousettus aegyptiacus* was taken from bats kept at the Lubee Bat Conservancy, a USDA registered facility, in Gainesville, Florida. The bats are group-housed in twelve 1068 sq. ft. enclosures with indoor temperature-controlled roosting areas and outdoor flight rooms and are fed a diet of fruit, vegetables and nutritional supplements. Wing tissue biopsies are periodically taken from individually marked animals and kept at -20°C in 95% ethanol. The majority of 243 samples from these species were taken from animals that were born in captivity. DNA was extracted with a Zymo miniprep plus kit.

Wing tissue samples were taken from captive *Carollia perspicillata* housed in a tropical zoo (Papiliorama, Kerzers FR, Switzerland). Approximately 400 bats roost in an artificial cave kept on a reversed light cycle and are fed twice a night with a fruit-based diet. Since 2011, the population has been monitored by capturing individuals using a harp-trap placed at the entrance to the cave. Forearm length, body weight, reproductive status and tooth-wear are recorded from every captured individual. At first capture, individuals are marked on the forearms with a unique combination of three colored plastic rings (A.C.Hughes, UK, size

XB). Between July and November 2018, 3mm biopsies were punched on the patagium and hermetically stored in silica gel. Based on the date of first capture and tooth-wear score, the age of each individual sampled was estimated [66]. DNA was extracted with a Zymo miniprep plus kit.

Biopsy punches (2 or 3 mm) were taken from the wing of captive common vampire bats, *Desmodus rotundus,* between 2010 and 2014 [for husbandry details see 67]. Bats were housed in flight cages (3 x 2 x 1.5 m) as a captive group at the Cranbrook Institute of Science (24-39 bats, Bloomfield Hills, MI, USA) or at the University of Maryland (7 bats, University of Maryland Institutional Animal Care and Use Committee protocol R-10–63). Age was determined based on zoo birth records. Individuals were born at the Houston Zoo, Cincinnati Zoo, Chicago Brookfield Zoo, or the Cranbrook Institute of Science. Tissue samples were stored in 95% ethanol prior to DNA extraction using a Qiagen DNeasy kit. DNA extracts were frozen for long-term storage at -80°C. Live animal procedures conformed to the American Society of Mammalogists guidelines and was approved by the University of Maryland Institutional Animal Care and Use Committee (protocol R-10-63).

Wing tissues were sampled in August 2018 and 2019 with a 3 mm biopsy punch from the wing of captive big brown bats (*Eptesicus fuscus*) of known age [68, 69]. The Cooper Laboratory at Northeast Ohio Medical University (NEOMED; Rootstown, Ohio) maintains [70] a colony of known-aged big brown bats transferred from a colony previously maintained by Dr. Ellen Covey at the University Washington. This colony was started in 2005 with bats caught in North Carolina and were banded according to year of capture or birth. These bats underwent natural hibernation and were exclusively fed an *ab libitum* diet of fresh water and mealworms (*Tenebrio molitor*) of known nutrient content. In 2014 bats were transported to

NEOMED and are now housed indoors on a 12 h light/dark cycle and fed the same *ab libitum* fresh water and mealworm diet. Tissue samples were stored frozen at -80°C in DNA Shield prior to DNA extraction with a Zymo miniprep plus kit.

During July 2019, wing membrane samples were obtained from subadult or adult female and subadult male lesser long-nosed bats, *Leptonycteris yerbabuenae,* with a 4 mm biopsy punch at the entrance of the Pinacate Cave in the Reserva de la Biosfera el Pinacate y Gran Desierto de Altar (31°38'51.6" N, 113°28'53.5" W), Sonora, Mexico. Bats were captured using mist nets (Avinet models: TB02, TB06, TB012; Portland, Maine, USA) set outside caves just prior to when bats emerged to forage. Individuals were sexed, weighed and the forearm measured. To discriminate subadults from adults, age was determined by the degree of fusion of the epiphyses at the metacarpal–phalangeal joint. Tissue samples were stored in DNA/RNA Shield buffer (Zymo Scientific, Irvine, CA 92614, U.S.A.). DNA was extracted with a Zymo miniprep plus kit. Bat tissue samples were collected under permit SGPA/DGVS/06361/17 issued to R. A. Medellín by The Ministry of Environment and Natural Resources.

Samples of velvet free-tailed bats, *Molossus molossus*, come from a long-term study [71-73] in Gamboa, Panama (09°07’ N 79°41’ W), where the bats roost in crevices in houses. We captured social groups with mist nets (Ecotone, Gydnia, Poland) at the entrance of roosts during evening emergence and individually marked all bats with a subcutaneous passive integrated transponder (Trovan ID-100, Euro ID, Weilerswist, Germany) at first capture. Wing tissue samples were taken with a 3 mm biopsy punch and stored in 96% ethanol until DNA extraction using a Zymo miniprep kit. Capture and handling of animals were carried out under permits from the Autoridad Nacional del Ambiente in Panama with approval from the

Institutional Animal Care and Use Committee of the Smithsonian Tropical Research Institute (2012-0505-2015).

Little brown bats, *Myotis lucifugus*, were captured as they departed from an attic maternity colony in Chestertown, Maryland, in September 1996. Captured bats were weighed, measured and banded with individually marked bands. Young of the year were identified by their weight and absence of tooth wear. Wing membrane biopsies were taken and stored in a 5M NaCl with 20% dimethyl sulfoxide solution and kept frozen at -80°C. DNA was extracted with a Zymo miniprep plus kit. Bat capture and handling was approved by the Maryland Department of Natural Resources.

Wing tissue samples were taken from greater mouse-eared bats, *Myotis myotis*, between 2013 and 2018 as part of a long-term mark-recapture study conducted by Bretagne Vivante in Brittany, France [74, 75]. Bats were caught using modified harp traps as they left the roost. Individuals at first capture are fitted with PIT tags to facilitate identification on subsequent recaptures. Measurements taken from each individual include sex, forearm length, weight and transponder number. Age class (juvenile or adult) is determined by examining the degree of the epiphyseal closure of the metacarpal-phalangeal joints [76]. Wing biopsies were taken with a 3 mm biopsy punch, flash frozen and stored in liquid nitrogen prior to extraction. All procedures were conducted with full ethical approval and permission (AREC-13-38-Teeling) awarded by the University College Dublin ethics committee. DNA was extracted from wing biopsies using a Promega Wizard SV DNA extraction kit (catalog no. A2371) or the Qiagen DNeasy Blood and Tissue kit (Qiagen). Extractions carried out with the Promega kit were partially automated using a Hamilton STAR Deck liquid handling robot.

Adult and juvenile Mexican fishing bats, *Myotis vivesi*, were captured by gloved hand from roosts in talus slopes on Isla Partida Norte in the Gulf of California, Mexico (29°03'N, 113°00'W) during the day between 2015 and 2018 [77, 78]. Individuals were measured and banded with numbered metal bands on their forearms for identification upon recapture. In 2018 wing tissue was taken with a 3 mm biopsy punch and preserved in Zymo DNA shield. Bat capture and handling were conducted under permits #7668–15 and 2492–17 from Dirección General de Vida Silvestre, and permits #17–16 and 21–17 from Secretaría de Gobernación, and the University of Maryland Institutional Animal Care and Use Committee protocols FR-15-10 and FR-18-20.

Common noctules, *Nyctalus noctula*, were captured as part of a long-term study [79-81] at the Seeburgpark in Kreuzlingen, Switzerland (47.649928° N, 9.186123° E) where bats regularly roost in boxes. Each bat was marked with a subcutaneous pit-tag (ID100; Euro ID, Weilerswist, Germany) injected under the dorsal skin. Wing tissue samples were taken with a 3 mm biopsy punch and stored in 96% ethanol until DNA extraction using a Zymo miniprep kit. All handling and sampling of the bats in Switzerland was approved by the Veterinäramt Thurgau (permit FIBL1/12).

Wing tissue samples were taken in September 2018 from lesser spear-nosed bats, *Phyllostomus discolor*, kept in a breeding colony in the Department Biology II of the Ludwig-Maximilians-University in Munich. In this colony animals were kept under semi-natural conditions (12 h day/night cycle, 65 to 70 % relative humidity, 28°C) with free access to food and water. The license to keep and breed *P. discolor* was issued by the German Regierung von Oberbayern. Under German Law on Animal Protection a special ethical approval is not needed for wing tissue collection. Wing tissue was stored in RNAlater until DNA was

extracted using QIAamp® MinElute columns following the manufacturer's instructions. The samples were eluted in 50µl of molecular grade water and concentrated to reduce their volume by approximately 50% using a Speedvac, with the following settings: duration 20 minutes, temperature in the chamber 30°C, H_2O (water) mode.

Greater spear-nosed bats, *Phyllostomus hastatus,* were captured and sampled between 1990 and 2018 in Trinidad, Lesser Antilles [82-85]. Most often, harem groups, which include one adult male plus 15-20 lactating females with pups, were captured during the day from within a solution depression in the ceiling of either Tamana (10.4711°N, 61.1958°W), Caura (10.7019°N, 61.3614°W), or Guanapo cave (10.6942°N, 61.2654°W) using a bucket trap. Captured bats were sexed, measured for size, weight, and tooth wear, and individually marked with stainless steel numbered bands. Age was determined exactly for adults that were recaptured after being banded as pups. Wing biopsy punches (4 mm) were stored frozen at -80°C in either a 5M NaCl with 20% dimethyl sulfoxide solution or Zymo DNA Shield prior to DNA extraction using a Qiagen Puregene or Zymo miniprep plus kit. Frozen samples were selected to maximize the number of known-age individuals with approximately equal numbers at all ages. Animal handling methods follow guidelines by the American Society of Mammalogists and were approved by the University of Maryland Institutional Animal Care and Use Committee (protocols R-91-33, R-94-25, R-01-07, R-11-21, R-13-77) under licenses from the Forestry Division of the Ministry of Agriculture, Land and Fisheries, Trinidad and Tobago.

Wing tissue samples were taken from greater horseshoe bats, *Rhinolophus ferrumequinum*, by using 3 mm biopsy punches between 2016 and 2018 from wild female bats as part of a long-term study at a maternity colony in Gloucestershire, UK [86-88]. Bats

were captured at the roost with hand nets, and all individuals were weighed, ringed with stainless-steel rings and morphometric data such as forearm length recorded. All bats studied were first marked as infants, so we could be certain of their age. Bats were aged between 1-21 years, with the 40 individuals selected in a fairly even manner across this age span. All procedures were conducted under licenses (Natural England 2015-11974-SCI-SCI; 2016-25216-SCI-SCI; 2017-31148-SCI-SCI) issued to Gareth Jones, with tissue biopsy additionally licensed under Home Office Project Licenses (PPL 30/3025 prior to 2018; P307F1428 from 2018 onwards) and Home Office personal licences. Tissue samples were stored in silica gel beads and then transferred to a -20C freezer for long-term storage. DNA was extracted from wing biopsies using a Promega Wizard SV DNA extraction kit or a Qiagen DNeasy Blood and Tissue kit. Extractions carried out with the Promega kit were partially automated using a Hamilton STAR Deck liquid handling robot but otherwise followed manufacturer's instructions.

Samples of proboscis bats, *Rhynchonycteris naso,* came from a long-term study between 2005 and 2016 at La Selva Biological Station in Costa Rica (10° 25´ N, 84° 00´W) [86-88]. Bats were mist-netted in the vicinity of their roosts. Wing tissue was sampled with a 4 mm biopsy punch, individuals were marked with colored plastic bands, sexed, measured and age class determined (juvenile: 0-4 months, subadult: 5-10 months, or adult>10 months) [89]. Age was determined exactly for individuals that were banded as pups and recaptured as adults. Ethanol (80%) was used to preserve tissue samples, and a salt–chloroform procedure or Qiagen BioSprint 96 DNA Blood Kit was used for DNA isolation [89, 90].

Samples of greater sac-winged bats, *Saccopteryx bilineata* came from long-term studies in Costa Rica (n = 21 from La Selva Biological Station,10° 25´ N, 84° 00´W and n = 6

from Santa Rosa National Park, 10° 53′ N, 85° 46′ W) and Panama (n = 4 from the Biological Station Barro Colorado Island (BCI) of the Smithsonian Tropical Research Institute, 9° 9′ N/79° 51′ W) between 1994 and 2016 [91, 92]. Bats were captured with mist nets when entering or leaving their day roosts, individually banded with two coloured plastic bands on their forearms, and a wing tissue biopsy sample (4mm) preserved in 80% ethanol was taken. Age was determined exactly for individuals that were banded as pups and recaptured as adults. DNA was extracted with a salt-chloroform procedure or with the Qiagen BioSprint 96 DNA Blood Kit [91, 93].

Mexican free-tailed bats, *Tadarida brasiliensis*, are housed at Bat World Sanctuary, a licensed non-profit bat rehabilitation facility and accredited sanctuary in Weatherford, Texas. Most individuals sampled were rescued as pups, although some were rescued as adults, making their exact age unknown. Individuals are group housed in large indoor enclosures. Wing membrane biopsies (4 mm) were collected in August 2019 and stored in Zymo DNA Shield until DNA was extracted using a Zymo miniprep plus kit.

After extraction DNA concentration was estimated with a QuBit and samples were concentrated, if necessary, to reach a minimum of 10 ng/µl in 20 µl. To estimate rates of methylation we limit analyses to the 23 species for which we had more than 10 samples from known-aged individuals. Maximum lifespan for each species was obtained from [1] or from captivity records (Supplementary Table 1).

DNA methylation profiling

DNA methylation was quantified using a custom Infinium methylation array, "HorvathMammalMethylChip40" that was designed using an alignment of 62 mammalian

species genomes to identify 35,500 highly conserved 50 bp sequences with a terminal CpG site. Five bat genomes, *Pteropus vampyrus, P. alecto, Eptesicus fuscus, Myotis davidii* and *M. lucifugus,* were included in the alignment. In addition, the chip contains two thousand probes selected from human biomarker studies.

Bisulfite conversion of DNA samples using the Zymo EZ DNA Methylation Kit (ZymoResearch, Orange, CA, USA), as well as subsequent hybridization and scanning (iScan, Illumina), were performed according to the manufacturers' protocols by applying standard settings. DNA methylation levels (β values) were determined by calculating the ratio of intensities between methylated (signal A) and unmethylated (signal B) sites. Specifically, the β value was calculated from the intensity of the methylated (M corresponding to signal A) and unmethylated (U corresponding to signal B) sites, as the ratio of fluorescent signals $\beta = Max(M,0)/[Max(M,0) + Max(U,0) + 100]$. Thus, β values range from 0 (completely unmethylated) to 1 (completely methylated). The SeSaMe method [94] was used to normalize β values for each probe.

Probe mapping and annotation

We used sequences and annotations for ten bat genomes (Supplementary Table 3), which include six recently published reference assemblies [19], to locate each 50 bp probe on the array. The alignment was done using the QUASR package [95] with the assumption for bisulfite conversion treatment of the genomic DNA. For each species' genome sequence, QUASR creates an in-silico-bisulfite-treated version of the genome. The set of nucleotide sequences of the designed probes, which includes degenerate base positions due to the bisulfite conversion, was expanded into a larger set of nucleotide sequences representing

every possible combination of degenerate bases. We then ran QUASR (a wrapper for Bowtie2) with parameters -k 2 --strata --best -v 3 and bisulfite = "undir" to align the enlarged set of probe sequences to each prepared genome. From these files, we collected only alignments where the entire length of the probe perfectly matched to the genome sequence (i.e. the CIGAR string 50M and flag XM=0).

Following the alignment, the CpGs were annotated based on the distance to the closest transcriptional start site using the Chipseeker package [96]. A gff file with these was created using these positions, sorted by scaffold and position, and compared to the location of each probe in BAM format. We report probes whose variants only mapped to one unique locus in a particular genome. Gene annotations for the ten bat genomes are available at http://hdl.handle.net/1903/26373.

Genomic location of each CpG was categorized as intergenic, 3' UTR, 5' UTR, promoter region (minus 10 kb to plus 1000 bp from the nearest TSS), exon, or intron. We identified X-linked probes in bat genomes by comparison to probes mapped to the X for the human genome, HG38. Tests for enrichment among genomic categories were performed with contingency or Fisher's Exact tests (FET) in JMP Pro v14.1 for the four species used to identify longevity-associated sites, i.e. one short-lived bat, *Molossus molossus,* and three long-lived bats, *Myotis myotis, Desmodus rotundus* and *Rhinolophus ferrumequinum*, representing four different bat families. While most sites map to the same nearest gene, some differences exist. In the text, we present enrichment results for the short-lived species, *M. molossus*, but provide parallel results in the Supplement for the long-lived species, *R. ferrumequinum, D. rotundus* and *M. myotis.*

Creation of epigenetic clocks using penalized regression

We developed epigenetic clocks for bat wing tissue by regressing chronological age on all CpGs that map to at least one of the ten bat genomes. To improve linear fit we transformed age to sqrt(age+1). Penalized regression models were created in the R package "glmnet" [97]. We investigated models produced by "elastic net" regression (alpha=0.5). The optimal penalty parameters in all cases were determined automatically by using a 10-fold internal cross-validation (cv.glmnet) on the training set. By definition, the alpha value for the elastic net regression was set to 0.5 (midpoint between Ridge and Lasso-type regression) and was not optimized for model performance. We performed two cross-validation schemes for arriving at unbiased estimates of the accuracy of the different DNAme based age estimators. One type consisted of leaving out a single sample (LOO) from the regression, predicting an age for that sample by regressing an elastic net on the methylation profiles of all other samples, and iterating over all samples. We conducted LOO analyses using all samples from all species, using all samples from each species, and using all samples from several species in the same genus (see Supplement for results of the latter two analyses). The second type consisted of leaving out a single species (LOSO) from the regression, thereby predicting the age of each sample using the data for all other species.

Identification of differentially methylated positions for age and longevity

To identify differentially methylated positions (DMPs) associated with age, we computed the Pearson correlation coefficient between methylation level (β) and transformed chronological age (sqrt(age +1)) for each of the 37,500 sites for the 19 species with 15 or more samples

(Supplementary Table 1). The significance of each site across species was then evaluated using Stouffer's unweighted z-test [98]. CpG sites were ranked by significance and the top 2000 sites were selected for subsequent analyses and are referred to as age DMPs. For probes with contrasting patterns in different species, direction was assigned based on the most frequent direction across species to ensure mean methylation rates are comprised of the same set of sites in each species. Because we used all sites on the array, some sites do not map to a unique position in all available bat genomes. The supplement indicates how many sites map to each of the four species with a genome that were used for identifying longevity DMPs.

To identify DMPs associated with longevity we compared methylation rates between three long-lived species (*R. ferrumequinum, D. rotundus,* and *M. myotis*) and two short-lived species (*M. molossus* and *L. yerbabuenae*). We chose these five species because they represent three independent lineages of increased longevity [1] and because high-quality genome assemblies are available for four of them [17]. We used a linear mixed-effects model (nlme) to model methylation level (β) in response to transformed chronological age (sqrt(age +1)), longevity category, and their interaction, with species included as a random effect. We defined probes as longevity-associated if the p-value of the interaction term was less than 0.05 after Benjamini-Yekutieli (BY) false discovery rate correction [16]. In this analysis, a positive interaction means a steeper positive slope for the short-lived species relative to the long-lived species. If the main effect of age is positive (hypermethylation) and the interaction is positive, then short-lived species are gaining methylation faster. If the main effect is negative and the interaction is negative, then short-lived species are losing methylation faster.

Phylogenetic analysis of bat longevity

Using phylogenetic generalized least squares regression (PGLS) we tested the effect of mean rate of methylation change on longevity using both the longevity quotient (LQ) and maximum longevity (log-transformed). LQ is the ratio of the observed species maximum lifespan to the maximum lifespan predicted for a nonflying placental mammal of the same body mass [1]. We present results for LQ in the text and for a model containing both log(maximum longevity) in Supplementary Table 2. For each species with at least 10 known-age samples, we calculated the mean rates of hypermethylation and hypomethylation using the top 2000 age-associated DMPs as described above. Hypermethylation and hypomethylation rates were tested separately. Log-transformed body mass [from 1] was included as a covariate in each log(maximum longevity) model. Phylogenetic relationships among bats are based on a recent maximum likelihood tree [14]. Models were fit via maximum likelihood using the "gls" function of the "nlme" package [99] and assume a Brownian model of trait evolution.

Probe and gene enrichment analyses

To determine how changes in methylation influence age and longevity, we conducted enrichment analyses on the CpG probes and on the genes nearest to them. We used eFORGE 2.0 [23, 98] to test for enrichment among age or longevity DMPs that either increase or decrease in methylation in comparison with five histone marks and 15 chromatin states mapped in cell lines by the Epigenomics Roadmap Consortium (http://www.ncbi.nlm.nih.gov/epigenomics). Bat wing tissue is unusual in that it contains epithelial skin, muscle, blood and elastin [53]. Consequently, we limited enrichment analyses to data from cell lines derived either from skin, blood or muscle. We also restricted the

analysis to probes mapped in a bat genome at least 1 kb apart. We used *Demodus rotundus* to provide a background probe set but obtained very similar results by using other bat genomes, e.g. *Eptesicus fuscus* or *Pteropus vampyrus,* available in eFORGE as backgrounds for the 37K array. We present enrichment values for each DMP set as the -log10 p binomial value and consider those outside the 95th percentile of the binomial distribution after correction for multiple testing [16] as significant.

We identified putative transcription factors that could utilize open chromatin and bind to the DNA by testing for enrichment in each DMP set for predicted binding sites among the probes on the 37K array. Binding sites were included if their FIMO (Find Individual Motif Occurrence)[100] p-value was less then 10e-5. We then used a hypergeometric test (phyper) to evaluate overlap between probe sets and transcription factor motifs obtained from four transcription factor databases: TRANSFAC [101], UniPROBE [102], HT-Selex[103], and JASPAR [104]. Redundant transcription factor motifs were then consolidated into clusters [cf. 105] to identify distinct transcription factors. Function was inferred using information derived primarily from studies in mouse and humans [106].

We used several approaches for determining the type and function of genes associated with age and longevity DMPs. First, we identified the gene (using human orthologs) with the nearest transcription start site to every mapped probe for each of the four species, *R. ferrumequinum, Desmodus rotundus, Myotis myotis* and *M. molossus,* used to identify longevity DMPs. We then used the subsequent lists of unique genes for each species as background for enrichment tests. While the number of probes near the same gene varies considerably, on average, each unique gene is near six probes. Thus, the number of unique genes with an identifiable human ortholog near a probe was near 5,000 with variation among

the four bat genomes (5262 in *R. ferrumequinum*, 5036 in *M. molossus*, 4935 in *M. myotis* and 4895 in *D. rotundus*) reflecting variation in the number of mapped probes (Supplementary Table 3). Given that the probes were designed to align to regions conserved across all mammals, we suspect some of the differences among species in gene associations reflect variation in genome assembly or annotation. In addition, an important caveat to keep in mind is that the CpGs on the array do not randomly sample the genome. Thus, even when we use mapped probes or the genes near them as background for enrichment tests, there is potential for bias given that the probes are in highly conserved regions. We assumed genes were associated with hypermethylated DMPs if they had more hypermethylated than hypomethylated sites nearest their transcription start site. We present results in the text for DMP-gene associations for *M. molossus* because it was the only short-lived species with a genome, but we summarize the DMP-gene associations for the other three species in Supplementary figures. Because we anticipated the mechanisms responsible for causing increases in methylation over time likely differs from those causing decreases, we conducted separate enrichment tests for genes with hypermethylated and hypomethylated sites associated with age and longevity using Panther v.14 [107, 108] in relation to biological process, molecular function, and protein class. We carried out enrichment tests using genes with DMPs in promoter regions because promoter regions showed enrichment for hypermethylated sites. We also used the significant age and longevity gene promoter lists to predict possible transcription factor regulators using BART, Binding Analysis for Regulation of Transcription [36], which correlates the cis-regulatory profile derived from a gene set to the genomic binding profiles of 918 transcription regulators using over 7000 human ChIP-seq datasets. We

report the Irwin-Hall P value, which indicates significance of the rank integrated over three test statistics [36].

In addition, we carried out three additional analyses to assess gene function. The first utilized a list of 394 genes associated with changes in methylation over the lifespan of dogs [18]. This recent study assayed over 50,000 CpG sites for 104 known-aged labrador dogs, and included methylation data from mice and humans, to identify 198 hypermethylated and 196 hypomethylated sites, with most of the hypermethylated sites near genes associated with anatomical development. By comparing gene lists, we identified the number of positive (and negative) methylated genes in the dog list that occur in the genome of each bat, and then used the number of genes in the bat, as well as the number of age-related genes in the bat and the number that overlap to calculate the probability associated with overlap in each methylation direction. We used the R program phyper to conduct a Fisher's Exact Test (FET) using the hypergeometric distribution.

The second test utilized a list of 576 genes that have been documented to mutate frequently in over 10,864 human tumor cases. We downloaded v1.25.1 (Aug 14, 2020) from the Genome Data Center of the National Cancer Institute (https://portal.gdc.cancer.gov). As with the dog age genes above, we calculated the probability of overlap between the cancer genes found in the genomes of each of four bat species and both the bat age and longevity gene lists using a FET.

The third test involved comparing a list of 4,723 innate immunity genes dowloaded from https://www.innatedb.com (Aug 14, 2020). As with the cancer gene list, we calculated the probability of overlap between the immunity genes found in the genome of the four bat genomes and both the bat age and longevity gene lists using a FET.

Acknowledgements

This work was supported by the Paul G. Allen Frontiers Group (PI SH) and an Irish Research Council Consolidator Laureate Award to ECT. We are grateful to the Neurogenomics Core at UCLA for laboratory assistance, to Amanda Lollar for providing *Tadarida* samples, and to Cold Spring Harbor for hosting the workshop that inspired this collaboration.

Author contributions

G.S.W., D.M.A. and S.H. conceived and designed the study. D.M.A., B.D.A., H.C.B., G.G.C., L.N.C., D.K.N.D., P.D., N.J.F., A.V.G., L.G., E.H., G.J., M.K., E.Z.L., F.M., R.A.M., M.N., B.P., M.L.P., R.D.R., E.C.T., S.C.V., G.S.W., and D.Z. provided or prepared samples. D.M.A., C.E.B, A.H., A.T.L., S.H., C.Z.L., J.A.R., G.S.W., Joseph Z. and Joshua Z. analyzed and interpreted data. G.S.W., D.M.A. and S.H. drafted the article. All authors provided comments to improve intellectual content and approve the final version.

Competing Interests

None declared.

Data availability

The design of the Illumina microarray (HorvathMammalMethylChip40) used to generate the DNA methylation data is available from the Gene Expression Omnibus (GEO) at NCBI as platform GPL28271. Gene annotations for the microarray for ten bat genomes are available

from the Digital Repository at the University of Maryland (DRUM) at http://hdl.handle.net/1903/26373. The normalized methylation values for each sample, along with the sample designations, are available from the corresponding author upon reasonable request.

Code availability

R code for implementing any of the analyses described in this paper is available upon reasonable request.

References

1. Wilkinson, G.S., and Adams, D.M. (2019). Recurrent evolution of extreme longevity in bats. Biol. Lett. *15*, 20180860.
2. Bocklandt, S., Lin, W., Sehl, M.E., Sanchez, F.J., Sinsheimer, J.S., Horvath, S., and Vilain, E. (2011). Epigenetic predictor of age. PloS one *6*, e14821.
3. Hannum, G., Guinney, J., Zhao, L., Zhang, L., Hughes, G., Sadda, S., Klotzle, B., Bibikova, M., Fan, J.B., Gao, Y., et al. (2013). Genome-wide methylation profiles reveal quantitative views of human aging rates. Mol. Cell *49*, 359-367.
4. Horvath, S. (2013). DNA methylation age of human tissues and cell types. Genome Biol *14*, R115.
5. Chen, B.H., Marioni, R.E., Colicino, E., Peters, M.J., Ward-Caviness, C.K., Tsai, P.C., Roetker, N.S., Just, A.C., Demerath, E.W., Guan, W., et al. (2016). DNA methylation-based measures of biological age: meta-analysis predicting time to death. Aging *8*, 1844-1865.
6. Marioni, R.E., Shah, S., McRae, A.F., Chen, B.H., Colicino, E., Harris, S.E., Gibson, J., Henders, A.K., Redmond, P., Cox, S.R., et al. (2015). DNA methylation age of blood predicts all-cause mortality in later life. Genome Biol *16*, 25.
7. Horvath, S., and Raj, K. (2018). DNA methylation-based biomarkers and the epigenetic clock theory of ageing. Nat. Rev. Genet. *19*, 371-384.
8. Brunet-Rossinni, A.K., and Wilkinson, G.S. (2009). Methods for age estimation and the study of senescence in bats. In Ecological and Behavioral Methods for the Study of Bats, T.H. Kunz and S. Parsons, eds. (Baltimore, MD.: Johns Hopkins University Press), pp. 315-325.
9. Ahn, M., Anderson, D.E., Zhang, Q., Tan, C.W., Lim, B.L., Luko, K., Wen, M., Chia, W.N., Mani, S., Wang, L.C., et al. (2019). Dampened NLRP3-mediated inflammation in bats and implications for a special viral reservoir host. Nat. Microbiol. *4*, 789-799.
10. Gorbunova, V., Seluanov, A., and Kennedy, B.K. (2020). The world goes bats: living longer and tolerating viruses. Cell Metab. *32*, 31-43.
11. Cole, J.J., Robertson, N.A., Rather, M.I., Thomson, J.P., McBryan, T., Sproul, D., Wang, T., Brock, C., Clark, W., Ideker, T., et al. (2017). Diverse interventions that extend mouse lifespan suppress shared age-associated epigenetic changes at critical gene regulatory regions. Genome Biol *18*, 58.
12. Maegawa, S., Lu, Y., Tahara, T., Lee, J.T., Madzo, J., Liang, S., Jelinek, J., Colman, R.J., and Issa, J.J. (2017). Caloric restriction delays age-related methylation drift. Nat. Comm. *8*, 539.
13. Lowe, R., Barton, C., Jenkins, C.A., Ernst, C., Forman, O., Fernandez-Twinn, D.S., Bock, C., Rossiter, S.J., Faulkes, C.G., Ozanne, S.E., et al. (2018). Ageing-associated DNA methylation dynamics are a molecular readout of lifespan variation among mammalian species. Genome Biol *19*, 22.
14. Amador, L.I., Arevalo, R.L.M., Almeida, F.C., Catalano, S.A., and Giannini, N.P. (2018). Bat systematics in the light of unconstrained analyses of a comprehensive molecular supermatrix. J. Mamm. Evol. *25*, 37-70.
15. Sen, P., Shah, P.P., Nativio, R., and Berger, S.L. (2016). Epigenetic mechanisms of longevity and aging. Cell *166*, 822-839.

16. Benjamini, Y., and Yekutieli, D. (2001). The control of the false discovery rate in multiple testing under dependency. Ann. Stat. *29*, 1165-1188.
17. Jebb, D., Huang, Z., Pippel, M., Hughes, G.M., Lavrichenko, K., Devanna, P., Winkler, S., Jermiin, L.S., Skirmuntt, E.C., Katzourakis, A., et al. (2020). Six reference-quality genomes reveal evolution of bat adaptations. Nature *583*, 578-584.
18. Wang, T., Ma, J., Hogan, A.N., Fong, S., Licon, K., Tsui, B., Kreisberg, J.F., Adams, P.D., Carvunis, A.R., Bannasch, D.L., et al. (2020). Quantitative translation of dog-to-human aging by conserved remodeling of the DNA methylome. Cell systems *11*, 176-185.
19. Ohm, J.E., McGarvey, K.M., Yu, X., Cheng, L., Schuebel, K.E., Cope, L., Mohammad, H.P., Chen, W., Daniel, V.C., Yu, W., et al. (2007). A stem cell-like chromatin pattern may predispose tumor suppressor genes to DNA hypermethylation and heritable silencing. Nat. Genet. *39*, 237-242.
20. Rakyan, V.K., Down, T.A., Maslau, S., Andrew, T., Yang, T.P., Beyan, H., Whittaker, P., McCann, O.T., Finer, S., Valdes, A.M., et al. (2010). Human aging-associated DNA hypermethylation occurs preferentially at bivalent chromatin domains. Genome research *20*, 434-439.
21. Breeze, C.E., Reynolds, A.P., van Dongen, J., Dunham, I., Lazar, J., Neph, S., Vierstra, J., Bourque, G., Teschendorff, A.E., Stamatoyannopoulos, J.A., et al. (2019). eFORGE v2.0: updated analysis of cell type-specific signal in epigenomic data. Bioinformatics *35*, 4767-4769.
22. Arthur, R.K., An, N., Khan, S., and McNerney, M.E. (2017). The haploinsufficient tumor suppressor, CUX1, acts as an analog transcriptional regulator that controls target genes through distal enhancers that loop to target promoters. Nucleic Acids Res *45*, 6350-6361.
23. Wilsker, D., Patsialou, A., Dallas, P.B., and Moran, E. (2002). ARID proteins: a diverse family of DNA binding proteins implicated in the control of cell growth, differentiation, and development. Cell Growth Differ. *13*, 95-106.
24. Engelmann, D., and Putzer, B.M. (2012). The dark side of E2F1: in transit beyond apoptosis. Cancer Res. *72*, 571-575.
25. Kim, W., Zhao, F., Wu, R., Qin, S., Nowsheen, S., Huang, J., Zhou, Q., Chen, Y., Deng, M., Guo, G., et al. (2019). ZFP161 regulates replication fork stability and maintenance of genomic stability by recruiting the ATR/ATRIP complex. Nat. Comm. *10*, 5304.
26. Zhou, P., Cowled, C., Mansell, A., Monaghan, P., Green, D., Wu, L., Shi, Z., Wang, L.F., and Baker, M.L. (2014). IRF7 in the Australian black flying fox, *Pteropus alecto*: evidence for a unique expression pattern and functional conservation. PloS one *9*, e103875.
27. Li, L., Wang, Y., Torkelson, J.L., Shankar, G., Pattison, J.M., Zhen, H.H., Fang, F., Duren, Z., Xin, J., Gaddam, S., et al. (2019). TFAP2C- and p63-dependent networks sequentially rearrange chromatin landscapes to drive human epidermal lineage commitment. Cell Stem Cell *24*, 271-284 e278.
28. Orso, F., Penna, E., Cimino, D., Astanina, E., Maione, F., Valdembri, D., Giraudo, E., Serini, G., Sismondi, P., De Bortoli, M., et al. (2008). AP-2alpha and AP-2gamma regulate tumor progression via specific genetic programs. Faseb J. *22*, 2702-2714.

29. Basyuk, E., Coulon, V., Le Digarcher, A., Coisy-Quivy, M., Moles, J.P., Gandarillas, A., and Journot, L. (2005). The candidate tumor suppressor gene ZAC is involved in keratinocyte differentiation and its expression is lost in basal cell carcinomas. Mol. Cancer Res. *3*, 483-492.
30. Poulin, H., and Labelle, Y. (2005). The PLAGL1 gene is down-regulated in human extraskeletal myxoid chondrosarcoma tumors. Cancer Lett. *227*, 185-191.
31. De Keersmaecker, K., Atak, Z.K., Li, N., Vicente, C., Patchett, S., Girardi, T., Gianfelici, V., Geerdens, E., Clappier, E., Porcu, M., et al. (2013). Exome sequencing identifies mutation in CNOT3 and ribosomal genes RPL5 and RPL10 in T-cell acute lymphoblastic leukemia. Nat. Genet. *45*, 186-190.
32. Shirai, Y.T., Mizutani, A., Nishijima, S., Horie, M., Kikuguchi, C., Elisseeva, O., and Yamamoto, T. (2019). CNOT3 targets negative cell cycle regulators in non-small cell lung cancer development. Oncogene *38*, 2580-2594.
33. Kumar, S. (2014). P53 induction accompanying G2/M arrest upon knockdown of tumor suppressor HIC1 in U87MG glioma cells. Mol. Cell. Biochem. *395*, 281-290.
34. Svedlund, J., Koskinen Edblom, S., Marquez, V.E., Akerstrom, G., Bjorklund, P., and Westin, G. (2012). Hypermethylated in cancer 1 (HIC1), a tumor suppressor gene epigenetically deregulated in hyperparathyroid tumors by histone H3 lysine modification. J. Clin. Endocrinol. Metab. *97*, E1307-1315.
35. Vaquerizas, J.M., Kummerfeld, S.K., Teichmann, S.A., and Luscombe, N.M. (2009). A census of human transcription factors: function, expression and evolution. Nat. Rev. Genet. *10*, 252-263.
36. Wang, Z., Civelek, M., Miller, C.L., Sheffield, N.C., Guertin, M.J., and Zang, C. (2018). BART: a transcription factor prediction tool with query gene sets or epigenomic profiles. Bioinformatics *34*, 2867-2869.
37. Lu, T., Aron, L., Zullo, J., Pan, Y., Kim, H., Chen, Y., Yang, T.H., Kim, H.M., Drake, D., Liu, X.S., et al. (2014). REST and stress resistance in ageing and Alzheimer's disease. Nature *507*, 448-454.
38. Razin, A., and Riggs, A.D. (1980). DNA methylation and gene function. Science *210*, 604-610.
39. Chen, Y., Breeze, C.E., Zhen, S., Beck, S., and Teschendorff, A.E. (2016). Tissue-independent and tissue-specific patterns of DNA methylation alteration in cancer. Epigenetics Chromatin *9*, 10.
40. Shemer, R., Birger, Y., Dean, W.L., Reik, W., Riggs, A.D., and Razin, A. (1996). Dynamic methylation adjustment and counting as part of imprinting mechanisms. Proc Natl Acad Sci U S A *93*, 6371-6376.
41. Gartler, S.M., and Riggs, A.D. (1983). Mammalian X-chromosome inactivation. Annu. Rev. Genet. *17*, 155-190.
42. Choi, J., Lyons, D.B., Kim, M.Y., Moore, J.D., and Zilberman, D. (2020). DNA methylation and histone H1 jointly repress transposable elements and aberrant intragenic transcripts. Mol. Cell *77*, 310-323 e317.
43. Klutstein, M., Nejman, D., Greenfield, R., and Cedar, H. (2016). DNA methylation in cancer and aging. Cancer Res. *76*, 3446-3450.
44. Unnikrishnan, A., Hadad, N., Masser, D.R., Jackson, J., Freeman, W.M., and Richardson, A. (2018). Revisiting the genomic hypomethylation hypothesis of aging. Ann. N. Y. Acad. Sci. *1418*, 69-79.

45. Petkovich, D.A., Podolskiy, D.I., Lobanov, A.V., Lee, S.G., Miller, R.A., and Gladyshev, V.N. (2017). Using DNA methylation profiling to evaluate biological age and longevity interventions. Cell Metab. *25*, 954-960 e956.
46. Stubbs, T.M., Bonder, M.J., Stark, A.K., Krueger, F., Team, B.I.A.C., von Meyenn, F., Stegle, O., and Reik, W. (2017). Multi-tissue DNA methylation age predictor in mouse. Genome Biol *18*, 68.
47. Thompson, M.J., vonHoldt, B., Horvath, S., and Pellegrini, M. (2017). An epigenetic aging clock for dogs and wolves. Aging *9*, 1055-1068.
48. Teschendorff, A.E., Menon, U., Gentry-Maharaj, A., Ramus, S.J., Weisenberger, D.J., Shen, H., Campan, M., Noushmehr, H., Bell, C.G., Maxwell, A.P., et al. (2010). Age-dependent DNA methylation of genes that are suppressed in stem cells is a hallmark of cancer. Genome Res. *20*, 440-446.
49. Christensen, B.C., Houseman, E.A., Marsit, C.J., Zheng, S., Wrensch, M.R., Wiemels, J.L., Nelson, H.H., Karagas, M.R., Padbury, J.F., Bueno, R., et al. (2009). Aging and environmental exposures alter tissue-specific DNA methylation dependent upon CpG island context. PLoS Genet. *5*, e1000602.
50. Day, K., Waite, L.L., Thalacker-Mercer, A., West, A., Bamman, M.M., Brooks, J.D., Myers, R.M., and Absher, D. (2013). Differential DNA methylation with age displays both common and dynamic features across human tissues that are influenced by CpG landscape. Genome Biol *14*, R102.
51. Ceballos-Vasquez, A., Caldwell, J.R., and Faure, P.A. (2015). Seasonal and reproductive effects on wound healing in the flight membranes of captive big brown bats. Biol Open *4*, 95-103.
52. Faure, P.A., Re, D.E., and Clare, E.L. (2009). Wound healing in the flight membranes of big brown bats. J. Mammal. *90*, 1148-1156.
53. Cheney, J.A., Allen, J.J., and Swartz, S.M. (2017). Diversity in the organization of elastin bundles and intramembranous muscles in bat wings. J. Anat. *230*, 510-523.
54. Conrad, L.G., Conrad, G.M., and Dawe, C.J. (1965). Cutaneous leiomyosarcoma in a long-eared bat, *Plecotus townsendii virginianus*, Handley. J. Natl. Cancer Inst. *35*, 95-101.
55. Andreasen, C.B., and Dulmstra, J.R. (1996). Multicentric malignant lymphoma in a pallid bat. J. Wildl. Dis. *32*, 545-547.
56. Beck, M., Beck, J., and Howard, E.B. (1982). Bile duct adenocarcinoma in a pallid bat (*Antrozeous pallidus*). J. Wildl. Dis. *18*, 365-367.
57. Chu, P.-Y., Zhuo, Y.-X., Wang, F.-I., Jeng, C.-R., Pang, V.F., Chang, P.-H., Chin, S.-C., and Liu, C.-H. (2012). Spontaneous neoplasms in zoo mammals, birds, and reptiles in Taiwan – a 10-year survey. Anim. Biology *62*, 95-110.
58. McKnight, C.A., Wise, A.G., Maes, R.K., Howe, C., Rector, A., Van Ranst, M., and Kiupel, M. (2006). Papillomavirus-associated basosquamous carcinoma in an Egyptian fruit bat (*Rousettus aegyptiacus*). J. Zoo Wildl. Med. *37*, 193-196.
59. Olds, J.E., Burrough, E.R., Fales-Williams, A.J., Lehmkuhl, A., Madson, D., Patterson, A.J., and Yaeger, M.J. (2015). Retrospective evaluation of cases of neoplasia in a captive population of Egyptian fruit bats (*Rousettus aegyptiacus*). J. Zoo Wildl. Med. *46*, 325-332.

60. Seim, I., Fang, X., Xiong, Z., Lobanov, A.V., Huang, Z., Ma, S., Feng, Y., Turanov, A.A., Zhu, Y., Lenz, T.L., et al. (2013). Genome analysis reveals insights into physiology and longevity of the Brandt's bat *Myotis brandtii*. Nat. Comm. *4*, 2212.
61. Huang, Z., Jebb, D., and Teeling, E.C. (2016). Blood miRNomes and transcriptomes reveal novel longevity mechanisms in the long-lived bat, *Myotis myotis*. BMC genomics *17*, 906.
62. Tisoncik, J.R., Korth, M.J., Simmons, C.P., Farrar, J., Martin, T.R., and Katze, M.G. (2012). Into the eye of the cytokine storm. Microbiol. Mol. Biol. Rev. *76*, 16-32.
63. Banerjee, A., Baker, M.L., Kulcsar, K., Misra, V., Plowright, R., and Mossman, K. (2020). Novel insights into immune systems of bats. Front. Immunol. *11*, 26.
64. Banerjee, A., Rapin, N., Bollinger, T., and Misra, V. (2017). Lack of inflammatory gene expression in bats: a unique role for a transcription repressor. Sci Rep *7*, 2232.
65. Sikes, R.S., and Gannon, W.L. (2011). Guidelines of the American Society of Mammalogists for the use of wild mammals in research. J. Mammal. *92*, 235-253.
66. Fasel, N., Saladin, V., and Richner, H. (2016). Alternative reproductive tactics and reproductive success in male *Carollia perspicillata* (Seba's short-tailed bat). J. Evol. Biol. *29*, 2242-2255.
67. Carter, G.G., and Wilkinson, G.S. (2016). Common vampire bat contact calls attract past food-sharing partners. Anim. Behav. *116*, 45-51.
68. Ball, H.C., Levari-Shariati, S., Cooper, L.N., and Aliani, M. (2018). Comparative metabolomics of aging in a long-lived bat: Insights into the physiology of extreme longevity. PloS one *13*, e0196154.
69. Ball, H.C., Moussa, F.M., Mbimba, T., Orman, R., Safadi, F.F., and Cooper, L.N. (2016). Methods and insights from the characterization of osteoprogenitor cells of bats (Mammalia: Chiroptera). Stem cell research *17*, 54-61.
70. Skrinyer, A.J., Faure, P.A., Dannemiller, S., Ball, H.C., Delaney, K.H., Orman, R., Stewart, M., and Cooper, L.N. (2017). Care and husbandry of the world's only flying mammals. Lab. Anim. Sci. Prof. *June*, 24-27.
71. Dechmann, D.K., Kranstauber, B., Gibbs, D., and Wikelski, M. (2010). Group hunting-a reason for sociality in molossid bats? PloS one *5*, e9012.
72. Dechmann, D.K., Ehret, S., Gaub, A., Kranstauber, B., and Wikelski, M. (2011). Low metabolism in a tropical bat from lowland Panama measured using heart rate telemetry: an unexpected life in the slow lane. J. Exp. Biol. *214*, 3605-3612.
73. Gager, Y., Gimenez, O., O'Mara, M.T., and Dechmann, D.K. (2016). Group size, survival and surprisingly short lifespan in socially foraging bats. BMC ecology *16*, 2.
74. Jebb, D., Foley, N.M., Whelan, C.V., Touzalin, F., Puechmaille, S.J., and Teeling, E.C. (2018). Population level mitogenomics of long-lived bats reveals dynamic heteroplasmy and challenges the free radical theory of ageing. Sci Rep *8*, 13634.
75. Foley, N.M., Petit, E.J., Brazier, T., Finarelli, J.A., Hughes, G.M., Touzalin, F., Puechmaille, S.J., and Teeling, E.C. (2020). Drivers of longitudinal telomere dynamics in a long-lived bat species, *Myotis myotis*. Mol. Ecol.
76. Kunz, T.H., and Anthony, E.L. (1982). Age estimation and post-natal growth in the bat *Myotis lucifugus*. J. Mammal. *63*, 23-32.
77. Egert-Berg, K., Hurme, E.R., Greif, S., Goldstein, A., Harten, L., Herrera, M.L., Flores-Martinez, J.J., Valdes, A.T., Johnston, D.S., Eitan, O., et al. (2018). Resource Ephemerality Drives Social Foraging in Bats. Curr. Biol. *28*, 3667-3673 e3665.

78. Hurme, E., Gurarie, E., Greif, S., Herrera, M.L., Flores-Martinez, J.J., Wilkinson, G.S., and Yovel, Y. (2019). Acoustic evaluation of behavioral states predicted from GPS tracking: a case study of a marine fishing bat. Mov Ecol *7*, 21.
79. Dechmann, D.K., Wikelski, M., Varga, K., Yohannes, E., Fiedler, W., Safi, K., Burkhard, W.D., and O'Mara, M.T. (2014). Tracking post-hibernation behavior and early migration does not reveal the expected sex-differences in a "female-migrating" bat. PloS one *9*, e114810.
80. Dechmann, D.K.N., Wikelski, M., Ellis-Soto, D., Safi, K., and O'Mara, M.T. (2017). Determinants of spring migration departure decision in a bat. Biol. Lett. *13*.
81. O'Mara, M.T., Wikelski, M., Kranstauber, B., and Dechmann, D.K.N. (2019). Common noctules exploit low levels of the aerosphere. R. Soc. Open Sci. *6*, 181942.
82. Adams, D.M., and Wilkinson, G.S. (2020). Male condition and group heterogeneity predict extra-group paternity in a Neotropical bat. Behav. Ecol. Sociobiol.
83. Bohn, K.M., Moss, C.F., and Wilkinson, G.S. (2009). Pup guarding by greater spear-nosed bats. Behav. Ecol. Sociobiol. *63*, 1693-1703.
84. Wilkinson, G.S., and Boughman, J.W. (1998). Social calls coordinate foraging in greater spear-nosed bats. Anim. Behav. *55*, 337-350.
85. Wilkinson, G.S., Carter, G.G., Bohn, K.M., and Adams, D.M. (2016). Non-kin cooperation in bats. Philos. Trans. R. Soc. Lond. B *371*, 20150095.
86. Carey, J.S., Danielsen, B., Gold, J.P., and Rossiter, S.J. (2005). Procedure rates and outcomes of coronary revascularization procedures in California and New York. The Journal of thoracic and cardiovascular surgery *129*, 1276-1282.
87. Foley, N.M., Hughes, G.M., Huang, Z., Clarke, M., Jebb, D., Whelan, C.V., Petit, E.J., Touzalin, F., Farcy, O., Jones, G., et al. (2018). Growing old, yet staying young: The role of telomeres in bats' exceptional longevity. Sci Adv *4*, eaao0926.
88. Ward, H.L., Ransome, R.D., Jones, G., and Rossiter, S.J. (2014). Determinants and patterns of reproductive success in the greater horseshoe bat during a population recovery. PloS one *9*, e87199.
89. Nagy, M., Günther, L., Knörnschild, M., and Mayer, F. (2013). Female-biased dispersal in a bat with a female-defence mating strategy. Mol. Ecol. *22*, 1733-1745.
90. Günther, L., Lopez, M.D., Knörnschild, M., Reid, K., Nagy, M., and Mayer, F. (2016). From resource to female defence: the impact of roosting ecology on a bat's mating strategy. R. Soc. Open Sci. *3*, 160503.
91. Nagy, M., Knörnschild, M., Voigt, C.C., and Mayer, F. (2012). Male greater sac-winged bats gain direct fitness benefits when roosting in multi- male colonies. Behav. Ecol. *23*, 597-606.
92. Knornschild, M., Bluml, S., Steidl, P., Eckenweber, M., and Nagy, M. (2017). Bat songs as acoustic beacons - male territorial songs attract dispersing females. Sci Rep *7*, 13918.
93. Heckel, G., Voigt, C.C., Mayer, F., and von Helversen, O. (1999). Extra-harem paternity in the white-lined bat *Saccopteryx bilineata* (Emballonuridae). Behav. *136*, 1173–1185.
94. Zhou, W., Triche, T.J., Jr., Laird, P.W., and Shen, H. (2018). SeSAMe: reducing artifactual detection of DNA methylation by Infinium BeadChips in genomic deletions. Nucleic Acids Res *46*, e123.

95. Gaidatzis, D., Lerch, A., Hahne, F., and Stadler, M.B. (2015). QuasR: quantification and annotation of short reads in R. Bioinformatics *31*, 1130-1132.
96. Yu, G., Wang, L.G., and He, Q.Y. (2015). ChIPseeker: an R/Bioconductor package for ChIP peak annotation, comparison and visualization. Bioinformatics *31*, 2382-2383.
97. Friedman, J., Hastie, T., and Tibshirani, R. (2010). Regularization paths for generalized linear models via coordinate descent. J. Stat. Software *33*, 1-22.
98. Stouffer, S.A., Suchman, E.A., DeVinney, L.C., Star, S.A., and Williams, R.M.J. (1949). The American Soldier, Vol 1: Adjustment during Army Life, (Princeton, NJ: Princeton University Press).
99. Pinheiro, J., Bates, D., DebRoy, S., Sarkar, D., and Team, R.C. (2019). nlme: Linear and Nonlinear Mixed Effects Models. R package version 3.1-143.
100. Grant, C.E., Bailey, T.L., and Noble, W.S. (2011). FIMO: scanning for occurrences of a given motif. Bioinformatics *27*, 1017-1018.
101. Matys, V., Kel-Margoulis, O.V., Fricke, E., Liebich, I., Land, S., Barre-Dirrie, A., Reuter, I., Chekmenev, D., Krull, M., Hornischer, K., et al. (2006). TRANSFAC and its module TRANSCompel: transcriptional gene regulation in eukaryotes. Nucleic Acids Res *34*, D108-110.
102. Hume, M.A., Barrera, L.A., Gisselbrecht, S.S., and Bulyk, M.L. (2015). UniPROBE, update 2015: new tools and content for the online database of protein-binding microarray data on protein-DNA interactions. Nucl. Acids Res. *43*, D117-122.
103. Yin, Y., Morgunova, E., Jolma, A., Kaasinen, E., Sahu, B., Khund-Sayeed, S., Das, P.K., Kivioja, T., Dave, K., Zhong, F., et al. (2017). Impact of cytosine methylation on DNA binding specificities of human transcription factors. Science *356*.
104. Fornes, O., Castro-Mondragon, J.A., Khan, A., van der Lee, R., Zhang, X., Richmond, P.A., Modi, B.P., Correard, S., Gheorghe, M., Baranasic, D., et al. (2020). JASPAR 2020: update of the open-access database of transcription factor binding profiles. Nucl. Acids Res. *48*, D87-D92.
105. Maurano, M.T., Haugen, E., Sandstrom, R., Vierstra, J., Shafer, A., Kaul, R., and Stamatoyannopoulos, J.A. (2015). Large-scale identification of sequence variants influencing human transcription factor occupancy in vivo. Nat. Genet. *47*, 1393-1401.
106. Lambert, S.A., Jolma, A., Campitelli, L.F., Das, P.K., Yin, Y., Albu, M., Chen, X., Taipale, J., Hughes, T.R., and Weirauch, M.T. (2018). The human transcription factors. Cell *172*, 650-665.
107. Mi, H., Muruganujan, A., Ebert, D., Huang, X., and Thomas, P.D. (2019). PANTHER version 14: more genomes, a new PANTHER GO-slim and improvements in enrichment analysis tools. Nucleic Acids Res *47*, D419-D426.
108. Mi, H., Muruganujan, A., Huang, X., Ebert, D., Mills, C., Guo, X., and Thomas, P.D. (2019). Protocol Update for large-scale genome and gene function analysis with the PANTHER classification system (v.14.0). Nature protocols *14*, 703-721.

Figure Legends

Fig. 1. Epigenetic clocks accurately predict chronological age of bats. a) Leave-one-out (LOO) cross-validation based on penalized regression of DNAm values gave a correlation of 0.95 with a median absolute error (MAE) of 0.72 years between observed and predicted (DNAmAge) age (after squareroot transform) for 26 bat species. b) Cross-validation analysis in which the data for one species was left out (LOSO) and ages are predicted for that species using a clock estimated with the remaining data. The resulting correlation between observed and predicted age is 0.8 (MAE = 1.3 years). Additional epigenetic clocks for individual species and genera are in Supplementary Fig. 1 and 2.

Fig. 2. Species longevity is predicted by mean rate of DNAm change. a) After controlling for phylogeny using phylogenetic generalized least squares regression, mean DNAm rate at 1175 hypermethylating age DMPs correlate with longevity (r = -0.704, t = -4.92, P = 7.26e-5), b) as does mean DNAm rate at 825 hypomethylating age DMPs (r = -0.679, t = -4.25, P = 3.55e-5). Species longevity is represented by the longevity quotient (LQ), which is the ratio of the observed species maximum lifespan to the maximum lifespan predicted for a nonflying placental mammal of the same body mass [1]. For example, the maximum longevity of *Myotis lucifugus* (10) is over six times longer than expected, while the maximum longevity of *Molossus molossus* (9) is equal to an average placental mammal of the same body size. The five species used for identifying longevity DMPs by difference in methylation rate are indicated by red triangles (long-lived) and blue triangles (short-lived).

Fig. 3. Differentially methylated positions (DMPs) for age and longevity are widely distributed and partially overlap. a) The top 2000 age-associated DMPs with positive (Pos) or negative (Neg) effects on DNAm are found on all *Rhinolophus ferrumequinum* chromosomes, although hypermethylated DMPs are underrepresented on chromosome 1 - syntenic with the human X. b) Longevity DMPs are also distributed across all *R. ferrumequinum* chromosomes. Darkened symbols indicate significance (BY 5% FDR). c) Age DMPs overlap 20% with hypermethylating (+) and hypomethylating (-) longevity DMPs. d) Number of unique genes nearest age and longevity DMPs for *M. molossus*. Sign on numbers in overlap region indicate methylation direction for age then longevity. Long-lived bat species show similar patterns (Supplementary Fig. 4d). e) Effect of DNAm change on age plotted against effect of DNAm change on longevity (see Methods) illustrates overlap among age and longevity sites. Significant sites are colored blue for age, purple for both age and longevity, and red for longevity. Symbols for the orthologous gene with the nearest transcription start site (TSS) to the DMP are indicated for a sample of extreme age and longevity DMPs. Bottom panels indicate DMPs that map to different genes in the short-lived species, *M. molossus,* than three long-lived species, *Desmodus rotundus*, *Myotis myotis*, and *R. ferrumequinum*, with the *M. molossus* gene indicated after /. Note that most extreme age and longevity DMPs in promoter regions (i.e. 1,000 to -10,000 bp from the tss) are in the upper right panel, i.e. nearest the same gene in multiple species.

Fig. 4. Age and longevity DMPs are enriched in promoter regions of genes associated with immunity and cancer. a) CpG annotation for the short-lived bat, *M. molossus,* in comparison to genome regions where probes map to the human genome (HG38) shows that

only 38% of probes that map to a promoter region in the bat also map to a promoter region in human (see also Supplementary Fig. 3). b) In contrast, CpG annotation comparison between two phylogenetically distant bat species, *M. molossus* and *R. ferrumequinum*, indicates greater probe conservation with respect to gene proximity (see also Supplementary Fig. 4). c) Age DMPs are highly enriched near promoter regions with over 95% exhibiting hypermethylation in *M. molossus* and other bats (Supplementary Fig. 4). d) Longevity DMPs are also enriched in promoter regions with over 80% exhibiting hypermethylation in *M. molossus* and other bats (Supplementary Fig. 4). e) Enriched biological processes for unique *M. molossus* genes from promoter regions are only significant for hypermethylating age and longevity DMPs. f) Enrichment analysis of protein class for unique *M. molossus* genes from promoter regions reveals significant enrichment of helix-turn-helix transcription factors (TF) only for hypermethylated DMPs associated with age and longevity. Cell color indicates significance (negative log P for GO terms with adjP < 10e-4) of enrichment in e) and f). g) Overlap between genes genes associated with longevity, innate immunity or frequently mutated in human tumors identified in *M. molossus*. Enrichment analyses using genome annotations from other bat species produce similar results (Supplement Fig. 5).

Fig. 5. Functional overlap analysis of DMPs reveals role for key transcriptional regulators. Histone marks for cell lines derived from skin, muscle or blood for DMPs mapped in *Desmodus rotundus* for (a) age and (b) longevity with bold symbols indicating significance (BY 5% FDR) and +/- indicating positive/negative rates of DNAm change. Predicted chromatin states for cell lines derived from skin, muscle or blood for DMPs for (c) age and (d) longevity. e) Transcription factor clusters enriched for hypermethylated (+) and

hypomethylated (-) age or longevity DMPs with cell color indicating significance (negative log P, adjP < 10e-4) of overlap with predicted transcription factor binding sites using a hypergeometric test. f) Top-ranked transcription factors associated with genes containing age or longevity DMPs in promoter regions in *M. molossus,* with integrative rank significance (see Methods) indicated as negative log P. Genes frequently mutated in human tumors are indicated by -c, and those involved in innate immunity by -i. Only genes with hypermethylated sites in promoter regions showed evidence of enrichment. Analyses using genome annotations from other bat species produce similar results (Supplement Fig. 5).

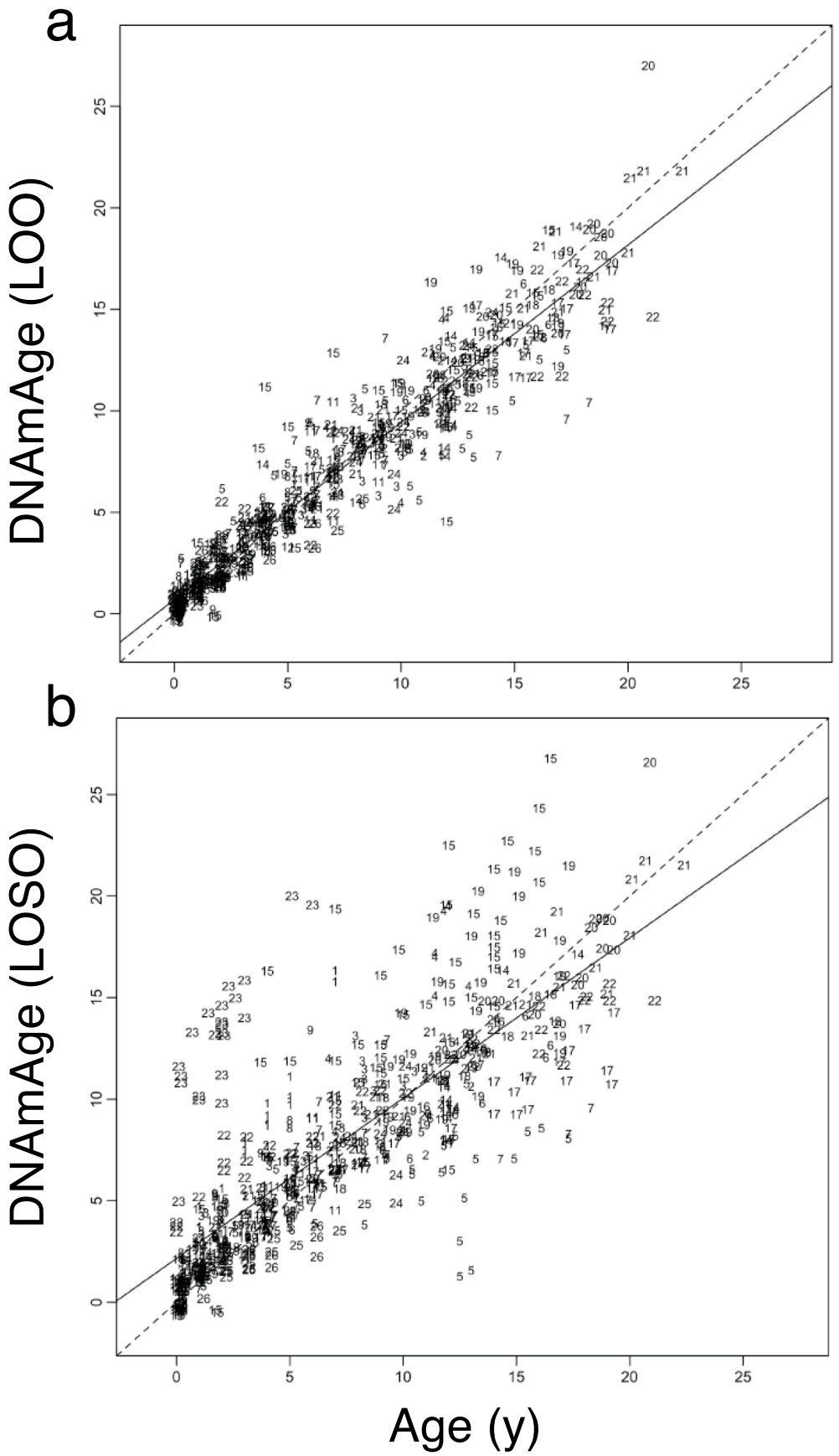

Bat species

1 *Antrozous pallidus*
2 *Artibeus jamaicensis*
3 *Carollia perspicillata*
4 *Cynopterus brachyotis*
5 *Desmodus rotundus*
6 *Eidolon helvum*
7 *Eptesicus fuscus*
8 *Leptonycteris curasoae*
9 *Molossus molossus*
10 *Myotis lucifugus*
11 *Myotis myotis*
12 *Myotis vivesi*
13 *Nyctalus noctule*
14 *Phyllostomus discolor*
15 *Phyllostomus hastatus*
16 *Pteropus giganteus*
17 *Pteropus hypomelanus*
18 *Pteropus poliocephalus*
19 *Pteropus pumilus*
20 *Pteropus rodricensis*
21 *Pteropus vampyrus*
22 *Rhinolophus ferrumequinum*
23 *Rhynchonycteris naso*
24 *Rousettus aegyptiacus*
25 *Saccopteryx bilineata*
26 *Tadarida brasiliensis*

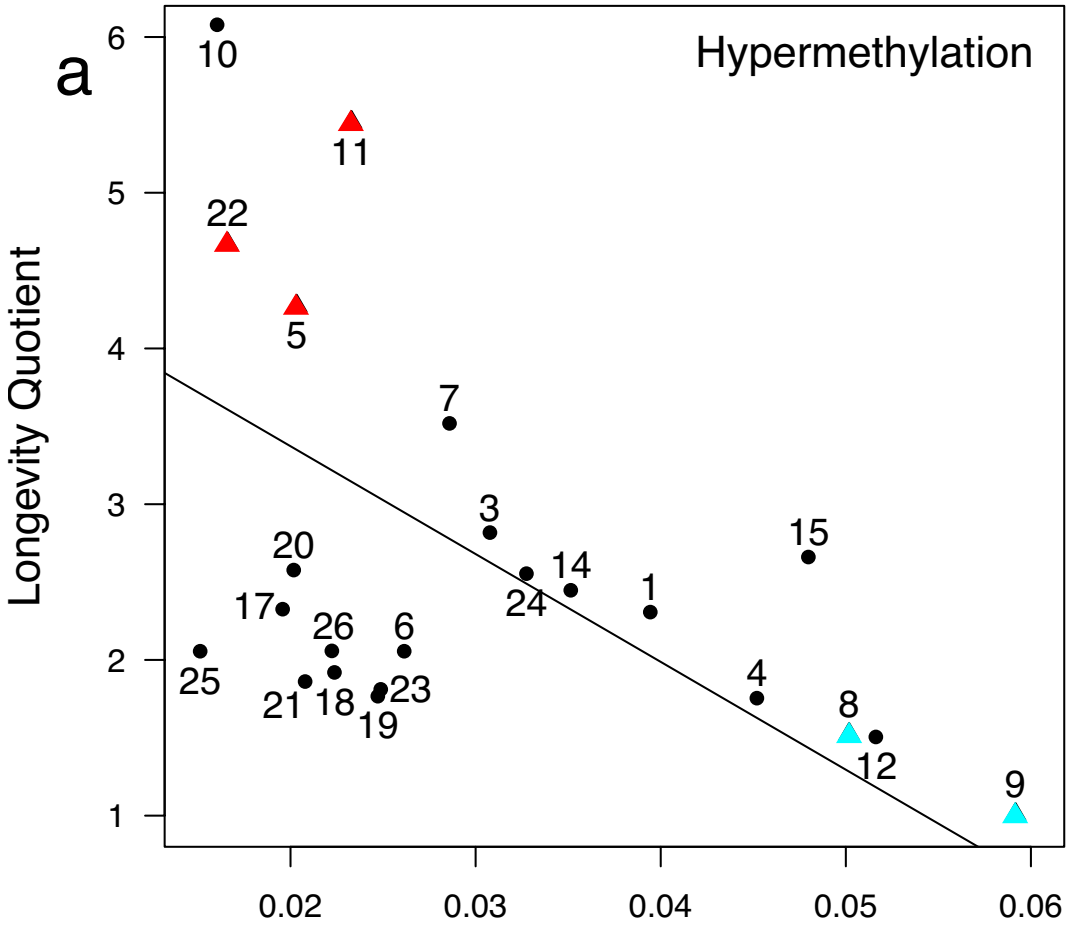

Bat species

1 *Antrozous pallidus*
2 *Artibeus jamaicensis*
3 *Carollia perspicillata*
4 *Cynopterus brachyotis*
5 *Desmodus rotundus*
6 *Eidolon helvum*
7 *Eptesicus fuscus*
8 *Leptonycteris curasoae*
9 *Molossus molossus*
10 *Myotis lucifugus*
11 *Myotis myotis*
12 *Myotis vivesi*
13 *Nyctalus noctule*
14 *Phyllostomus discolor*
15 *Phyllostomus hastatus*
16 *Pteropus giganteus*
17 *Pteropus hypomelanus*
18 *Pteropus poliocephalus*
19 *Pteropus pumilus*
20 *Pteropus rodricensis*
21 *Pteropus vampyrus*
22 *Rhinolophus ferrumequinum*
23 *Rhynchonycteris naso*
24 *Rousettus aegyptiacus*
25 *Saccopteryx bilineata*
26 *Tadarida brasiliensis*

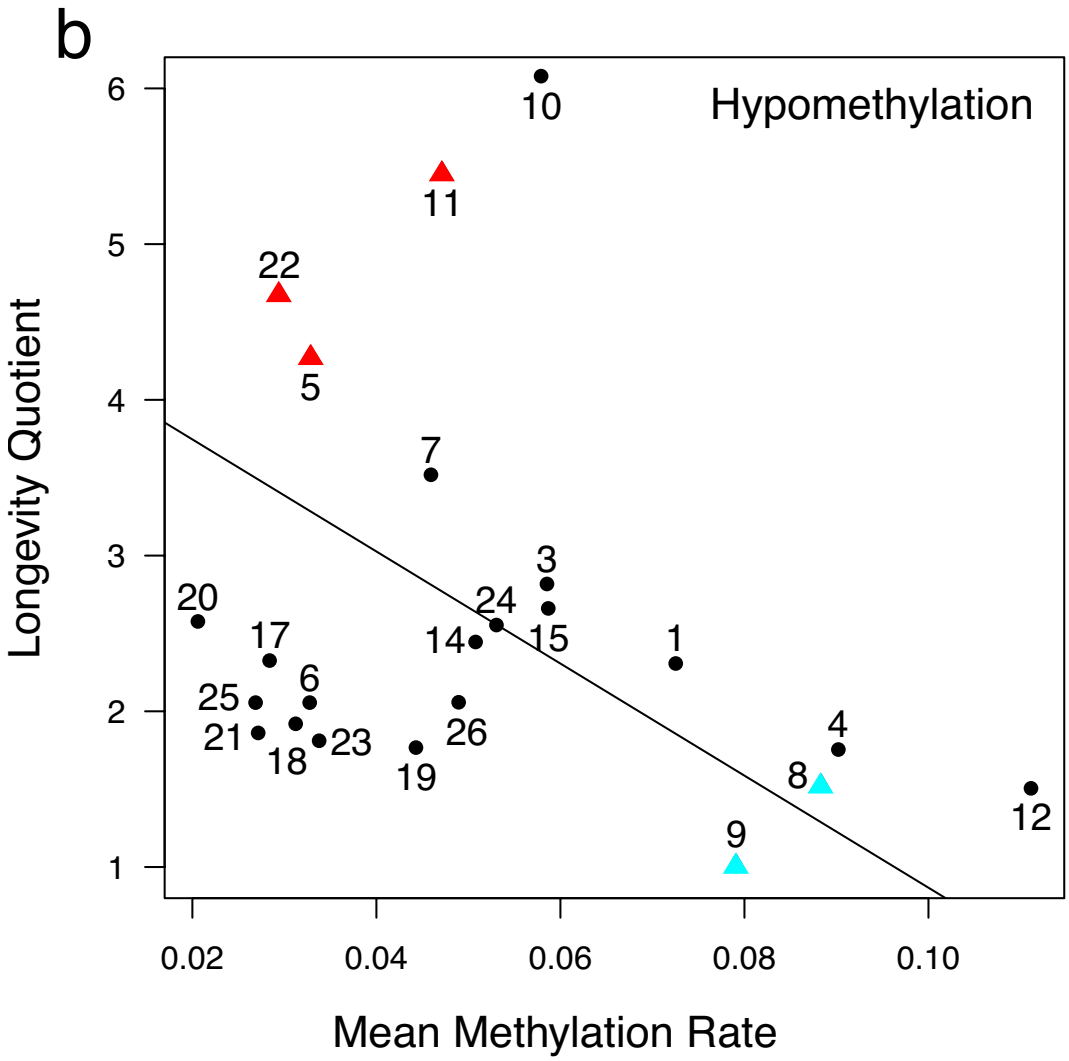

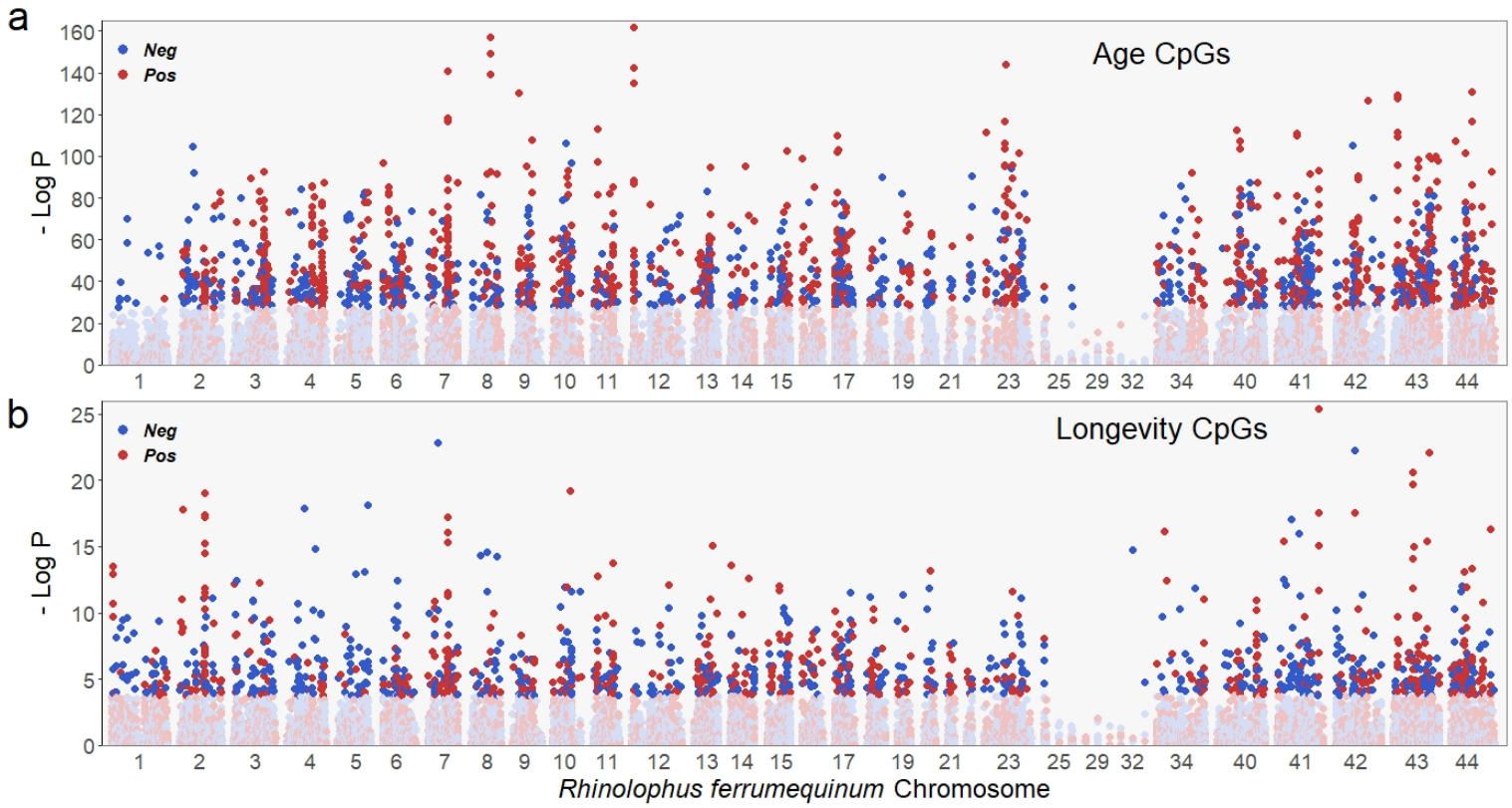
a
Neg
Pos
Age CpGs
- Log P
b
Neg
Pos
Longevity CpGs
- Log P
Rhinolophus ferrumequinum Chromosome

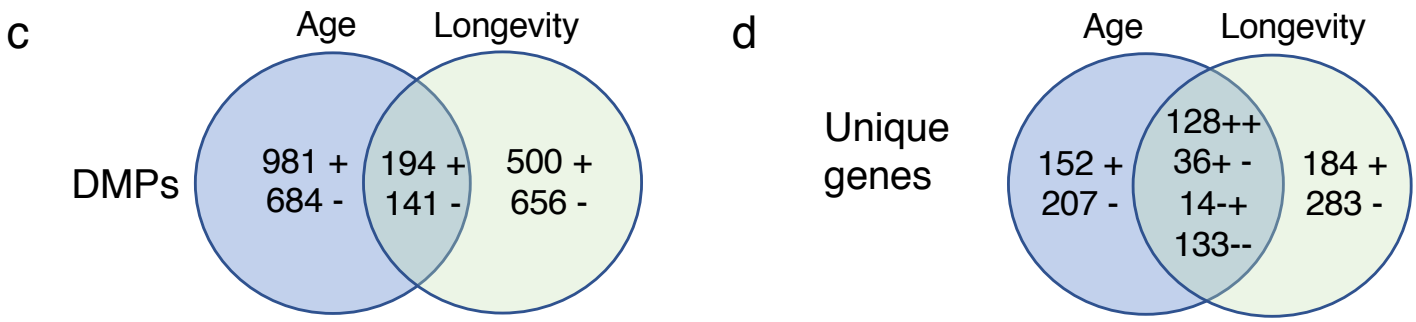
c
Age
Longevity
DMPs
981 +
684 -
194 +
141 -
500 +
656 -
d
Age
Longevity
Unique genes
152 +
207 -
128++
36+ -
14-+
133--
184 +
283 -

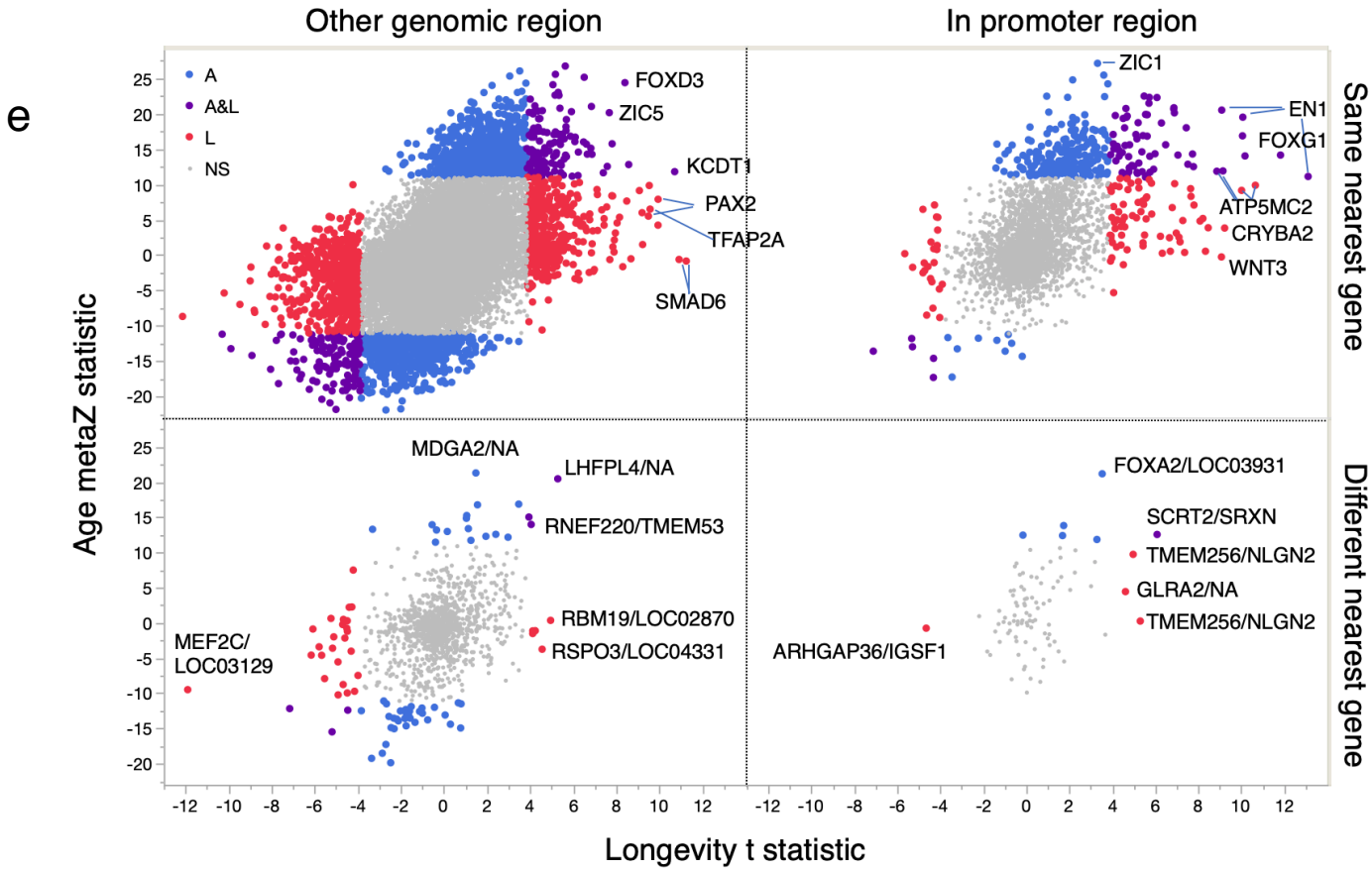
e
Other genomic region
In promoter region
A
A&L
L
NS
FOXD3
ZIC5
KCDT1
PAX2
TFAP2A
SMAD6
ZIC1
EN1
FOXG1
ATP5MC2
CRYBA2
WNT3
Same nearest gene
MDGA2/NA
LHFPL4/NA
RNEF220/TMEM53
RBM19/LOC02870
RSPO3/LOC04331
MEF2C/
LOC03129
FOXA2/LOC03931
SCRT2/SRXN
TMEM256/NLGN2
GLRA2/NA
TMEM256/NLGN2
ARHGAP36/IGSF1
Different nearest gene
Age metaZ statistic
Longevity t statistic

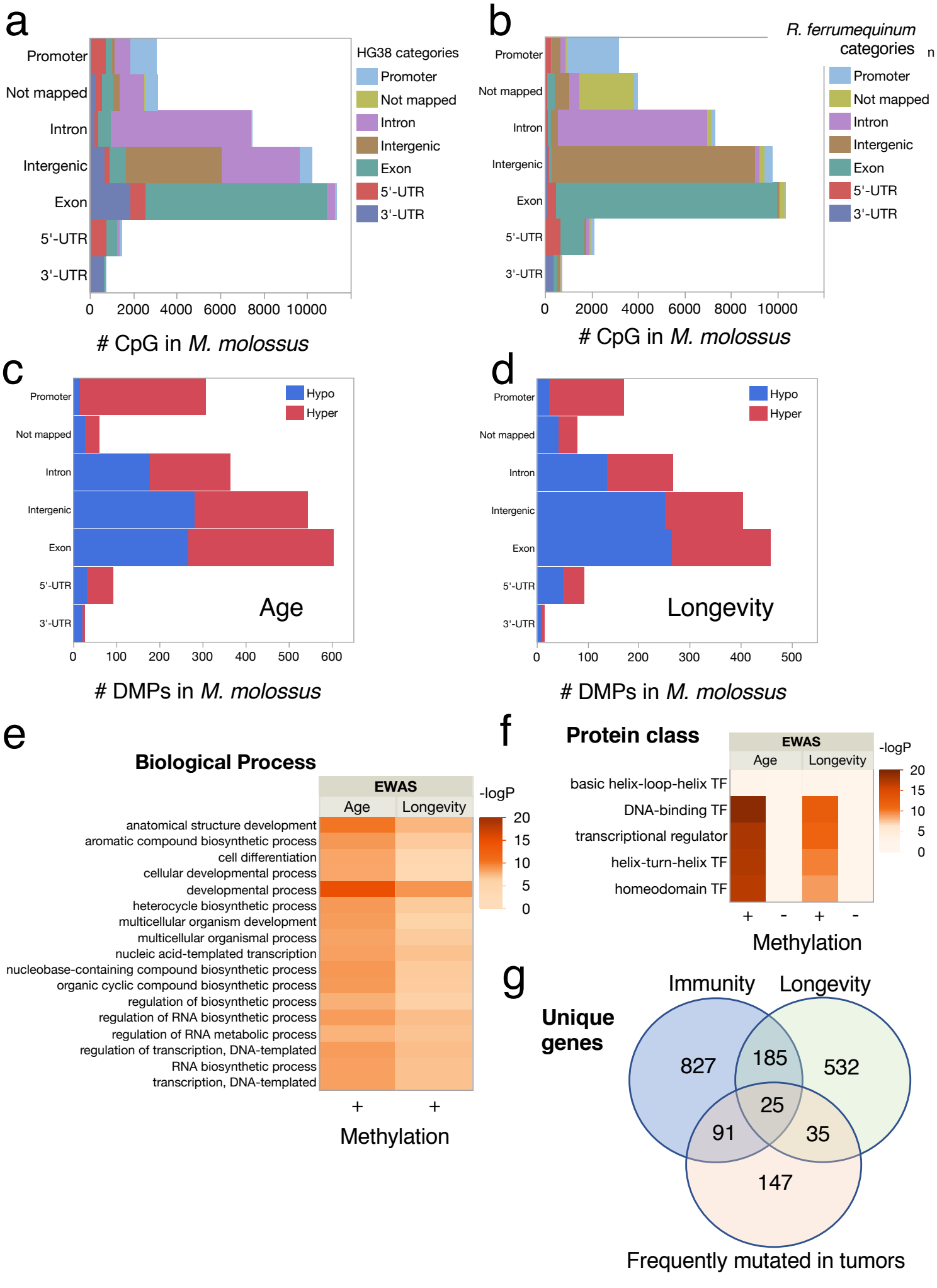
a
Promoter
Not mapped
Intron
Intergenic
Exon
5'-UTR
3'-UTR
0 2000 4000 6000 8000 10000
CpG in M. molossus
HG38 categories
Promoter
Not mapped
Intron
Intergenic
Exon
5'-UTR
3'-UTR
b
R. ferrumequinum categories
n
Promoter
Not mapped
Intron
Intergenic
Exon
5'-UTR
3'-UTR
0 2000 4000 6000 8000 10000
CpG in M. molossus
c
Hypo
Hyper
Age
0 100 200 300 400 500 600
DMPs in M. molossus
d
Hypo
Hyper
Longevity
0 100 200 300 400 500
DMPs in M. molossus
e
Biological Process
EWAS
Age
Longevity
-logP
20
15
10
5
0
anatomical structure development
aromatic compound biosynthetic process
cell differentiation
cellular developmental process
developmental process
heterocycle biosynthetic process
multicellular organism development
multicellular organismal process
nucleic acid-templated transcription
nucleobase-containing compound biosynthetic process
organic cyclic compound biosynthetic process
regulation of biosynthetic process
regulation of RNA biosynthetic process
regulation of RNA metabolic process
regulation of transcription, DNA-templated
RNA biosynthetic process
transcription, DNA-templated
+ +
Methylation
f
Protein class
EWAS
Age
Longevity
-logP
20
15
10
5
0
basic helix-loop-helix TF
DNA-binding TF
transcriptional regulator
helix-turn-helix TF
homeodomain TF
+ - + -
Methylation
g
Unique genes
Immunity
Longevity
827
185
532
25
91
35
147
Frequently mutated in tumors

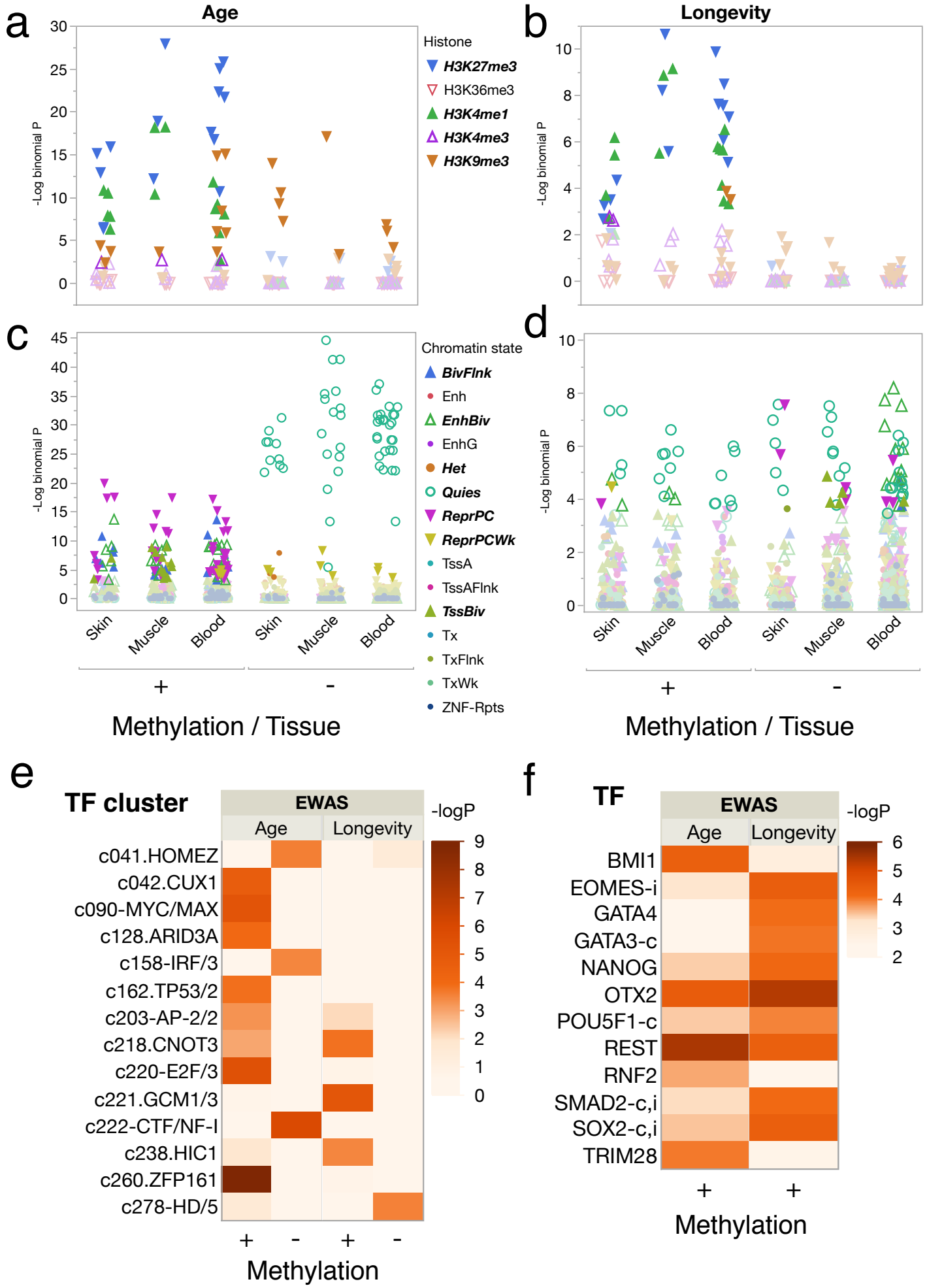
a
Age
-Log binomial P
Histone
H3K27me3
H3K36me3
H3K4me1
H3K4me3
H3K9me3
b
Longevity
-Log binomial P
c
-Log binomial P
Chromatin state
BivFlnk
Enh
EnhBiv
EnhG
Het
Quies
ReprPC
ReprPCWk
TssA
TssAFlnk
TssBiv
Tx
TxFlnk
TxWk
ZNF-Rpts
Skin
Muscle
Blood
Skin
Muscle
Blood
+
-
Methylation / Tissue
d
-Log binomial P
Skin
Muscle
Blood
Skin
Muscle
Blood
+
-
Methylation / Tissue
e
TF cluster
EWAS
Age
Longevity
-logP
c041.HOMEZ
c042.CUX1
c090-MYC/MAX
c128.ARID3A
c158-IRF/3
c162.TP53/2
c203-AP-2/2
c218.CNOT3
c220-E2F/3
c221.GCM1/3
c222-CTF/NF-I
c238.HIC1
c260.ZFP161
c278-HD/5
+
-
+
-
Methylation
f
TF
EWAS
Age
Longevity
-logP
BMI1
EOMES-i
GATA4
GATA3-c
NANOG
OTX2
POU5F1-c
REST
RNF2
SMAD2-c,i
SOX2-c,i
TRIM28
+
+
Methylation